

NATIONAL AERONAUTICS AND SPACE ADMINISTRATION

Technical Report No. 32-803

High-Energy Trajectories From Earth to Mars and Return

S. S. Dallas

FACILITY FORM 602

N66-15223

(ACCESSION NUMBER)

(THRU)

59

1

(PAGES)

(CODE)

CR 69221

30

(NASA CR OR TMX OR AD NUMBER)

(CATEGORY)

GPO PRICE \$ _____

CFSTI PRICE(S) \$ _____

Hard copy (HC) *3.00*

Microfiche (MF) *.50*

ff 653 July 65



**JET PROPULSION LABORATORY
CALIFORNIA INSTITUTE OF TECHNOLOGY
PASADENA, CALIFORNIA**

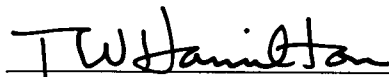
December 15, 1965

NATIONAL AERONAUTICS AND SPACE ADMINISTRATION

Technical Report No. 32-803

High-Energy Trajectories From Earth to Mars and Return

S. S. Dallas

A handwritten signature in dark ink, reading "T W Hamilton", is written over a horizontal line.

T. W. Hamilton, Manager
Systems Analysis Section

JET PROPULSION LABORATORY
CALIFORNIA INSTITUTE OF TECHNOLOGY
PASADENA, CALIFORNIA

December 15, 1965

Copyright © 1965
Jet Propulsion Laboratory
California Institute of Technology

Prepared Under Contract No. NAS 7-100
National Aeronautics & Space Administration

CONTENTS

I. Introduction	1
II. Trajectory Computation	2
A. Present Trajectory Design Technique	2
B. Round-Trip Trajectory Computing Program	2
C. Mathematical Limitations	2
III. Trajectories for the 1970-to-1980 Decade	3
A. Design Constraints	3
B. Degenerate Trajectories—Target Planet in Pseudo-opposition.	3
C. Out-of-the-Ecliptic Trajectories—Target Planet in Pseudo-conjunction	5
D. Theoretical Discussion	6
Nomenclature	15
References	17
Appendixes	
A. Calculation of Exact and Approximate Expressions for $(\Delta V)_T$	18
B. Plots of $(V_\infty)_T$ and $(\Delta V)_T$ vs Launch Date From the Earth in the Decade 1970 to 1980	21
C. Tabulation of Reasons for Peculiar Variations in Plots of $(V_\infty)_T$ and $(\Delta V)_T$ vs Launch Date From the Earth in the Decade 1970 to 1980	43

TABLES

1. Design constraints	3
2. Relative minimum $(V_\infty)_T$ for the decade 1970 to 1980	8
C-1. Reasons for the peculiar variations in Figs. B-2 through B-11 for the one-way time of flight of 30 days	44
C-2. Reasons for the peculiar variations in Figs. B-2 through B-11 for the one-way time of flight of 60 days	46
C-3. Reasons for the peculiar variations in Figs. B-2 through B-11 for the one-way time of flight of 120 days	48
C-4. Reasons for the peculiar variations in Figs. B-2 through B-11 for the one-way time of flight of 240 days	50

FIGURES

1. Trajectory profile	1
2. Heliocentric problem to be solved	3
3. Difference between direct and indirect rectilinear elliptic trajectories	4
4. Direct transfer orbit for planets just prior to pseudo-opposition, $\beta_{\delta} < 0$	4
5. Direct transfer orbit for planets just prior to pseudo-opposition, $\beta_{\delta} > 0$	4
6. Indirect transfer orbit for planets just after pseudo-opposition, $\beta_{\delta} < 0$	5
7. Out-of-the-ecliptic transfer orbit for planets just prior to pseudo-conjunction, $\beta_{\delta} > 0$	5
8. Out-of-the-ecliptic transfer orbit for planets just after pseudo-conjunction, $\beta_{\delta} > 0$	6
9. Dependence of the hyperbolic excess speed on the inclination of the transfer orbit	6
10. Total speed increment from Earth orbit to Mars orbit to Earth orbit vs the sum of geocentric and areocentric hyperbolic excess speeds	7
11. Dependence of the hyperbolic excess speed on the direction of the transfer orbit for pseudo-conjunction	10
12. Dependence of the hyperbolic excess speed on the direction of the transfer orbit for pseudo-opposition	12
B-1. Earth-Mars-Earth trajectories, 1970 to 1980, sum of geocentric and areocentric hyperbolic excess speeds vs launch date	21
B-2. Earth-Mars-Earth trajectories, 1970, sum of geocentric and areocentric hyperbolic excess speeds vs launch date	22
B-3. Earth-Mars-Earth trajectories, 1971, sum of geocentric and areocentric hyperbolic excess speeds vs launch date	23
B-4. Earth-Mars-Earth trajectories, 1972, sum of geocentric and areocentric hyperbolic excess speeds vs launch date	24
B-5. Earth-Mars-Earth trajectories, 1973, sum of geocentric and areocentric hyperbolic excess speeds vs launch date	25
B-6. Earth-Mars-Earth trajectories, 1974, sum of geocentric and areocentric hyperbolic excess speeds vs launch date	26
B-7. Earth-Mars-Earth trajectories, 1975, sum of geocentric and areocentric hyperbolic excess speeds vs launch date	27
B-8. Earth-Mars-Earth trajectories, 1976, sum of geocentric and areocentric hyperbolic excess speeds vs launch date	28

FIGURES (Cont'd)

B-9. Earth-Mars-Earth trajectories, 1977, sum of geocentric and areocentric hyperbolic excess speeds vs launch date	29
B-10. Earth-Mars-Earth trajectories, 1978, sum of geocentric and areocentric hyperbolic excess speeds vs launch date	30
B-11. Earth-Mars-Earth trajectories, 1979, sum of geocentric and areocentric hyperbolic excess speeds vs launch date	31
B-12. Earth-Mars-Earth trajectories, 1970, total speed increment from Earth orbit to Mars orbit to Earth orbit vs launch date	32
B-13. Earth-Mars-Earth trajectories, 1971, total speed increment from Earth orbit to Mars orbit to Earth orbit vs launch date	33
B-14. Earth-Mars-Earth trajectories, 1972, total speed increment from Earth orbit to Mars orbit to Earth orbit vs launch date	34
B-15. Earth-Mars-Earth trajectories, 1973, total speed increment from Earth orbit to Mars orbit to Earth orbit vs launch date	35
B-16. Earth-Mars-Earth trajectories, 1974, total speed increment from Earth orbit to Mars orbit to Earth orbit vs launch date	36
B-17. Earth-Mars-Earth trajectories, 1975, total speed increment from Earth orbit to Mars orbit to Earth orbit vs launch date	37
B-18. Earth-Mars-Earth trajectories, 1976, total speed increment from Earth orbit to Mars orbit to Earth orbit vs launch date	38
B-19. Earth-Mars-Earth trajectories, 1977, total speed increment from Earth orbit to Mars orbit to Earth orbit vs launch date	39
B-20. Earth-Mars-Earth trajectories, 1978, total speed increment from Earth orbit to Mars orbit to Earth orbit vs launch date	40
B-21. Earth-Mars-Earth trajectories, 1979, total speed increment from Earth orbit to Mars orbit to Earth orbit vs launch date	41

ABSTRACT

15223

The speed increment requirements are investigated for a spacecraft traveling (1) from a circular parking orbit about the Earth, (2) to the vicinity of the planet Mars, (3) into a circular parking orbit about Mars, (4) out of the circular parking orbit about Mars (after a stay time of 7 days), (5) to the vicinity of the Earth, and (6) back into the circular parking orbit about the Earth.

A three-dimensional analytic conic approximation to the accurate integrated trajectory is used in the analysis. This approximation is similar to the one used initially in the computation of one-way interplanetary trajectories.

The characteristics of the high-energy trajectories from Earth to Mars and return for the entire decade beginning January 1970 and ending January 1980 are investigated for four round-trip flight times. The four round-trip flight times (including a 7-day stay time at Mars) are 67, 127, 247, and 487 days. The one-way flight times of the departure and return trajectories are the same. The trajectories were computed by an IBM 7090 digital computer once for each day (zero hours GMT) in the decade. The energy information that is presented for the complete decade of launch dates can be used in parametric studies of advanced manned space flight missions to Mars. In addition, theoretical phenomena inherent in round-trip trajectories are discussed and explained; such phenomena include the occurrence of the out-of-the-ecliptic one-way trajectory or the nearly rectilinear one-way trajectory.

Author

I. INTRODUCTION

This Report presents information that can be used in parametric studies of possible advanced manned space flight missions to Mars and discusses phenomena inherent in round-trip trajectories. Figure 1 shows a simplified profile of a typical trajectory as studied in this Report. The Earth is shown at the time of launch and Mars is shown at the time of arrival. This type of representation is used throughout the Report. The spacecraft is initially assumed to be in a circular parking orbit about the Earth. The problem of placing the spacecraft into such an orbit is not considered in this analysis. The spacecraft is thrust into a transfer orbit to the vicinity of the planet Mars. At the appropriate distance from Mars, a retro-thrust is applied, placing the spacecraft in a circular parking orbit about Mars. The spacecraft remains in this parking orbit for 7 days and then is thrust into a transfer orbit returning to the vicinity of the Earth. At the appropriate distance from the Earth, a retro-thrust is applied, placing the spacecraft in a circular parking orbit about the Earth similar to the initial parking orbit. Figure 1 is not an actual trajectory profile as studied in this Report, for it shows coplanar planet orbits and neglects the motion of the planets during the 7-day stay at Mars.

Computations were made using a three-dimensional trajectory computing program, based upon the conic approximation theory, designed for the IBM 7090 digital computer.

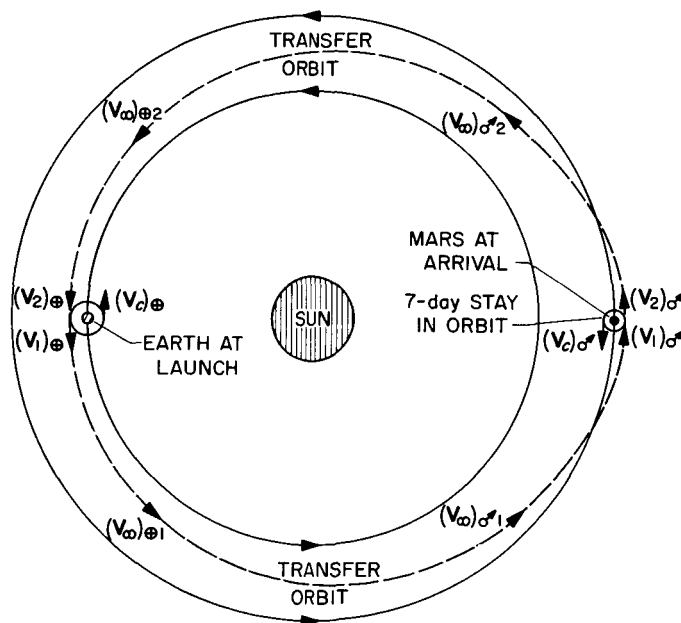


Fig. 1. Trajectory profile

II. TRAJECTORY COMPUTATION

The approximation to the accurate integrated transfer orbit* used in this analysis is the same as the approximation used in the computation of one-way interplanetary trajectories and is described in Ref. 1. Briefly, the approximation consists of three distinct phases of Keplerian motion: hyperbolic motion in the vicinity of the launch planet, Keplerian motion during flight when the Sun is the principal body of force (central body), and hyperbolic motion in the vicinity of the target planet. The central body in each phase is considered as a point mass, and the mass of the spacecraft is assumed to be negligibly small. The three-dimensional positions and velocities of the launch and target planets are obtained from the ephemeris tapes prepared at the Jet Propulsion Laboratory (JPL).

The trajectory computing program used was the heliocentric conic program also described in Ref. 1. The program begins by solving for the heliocentric transfer orbit that passes through the centers of the massless launch planet and target planet. The primary result obtained from the solution of the heliocentric transfer problem is the hyperbolic excess velocity vector relative to the launch planet. This vector is used as the starting point for the computation of the launch planetocentric hyperbola. In addition, the hyperbolic excess velocity vector, relative to the target planet, is computed. This trajectory computing program was written basically for unmanned one-way interplanetary trajectories. As a result, certain mathematical limitations and inefficiency exist when this program is used to study high-energy trajectories from Earth to Mars and return.

A. Present Trajectory Design Technique

The present technique for designing round-trip trajectories to the planets is to use a particular launch time and associated data as input into the heliocentric conic

program, which then computes a one-way departure trajectory, i.e., the trajectory from the initial launch planet to the target planet. The arrival time is then obtained from the departure trajectory. The stay time* is added to this date, resulting in the return launch date for the one-way return trajectory, i.e., the trajectory from the initial target planet to the initial launch planet. Putting this return launch date and associated data into the heliocentric conic program and interchanging the initial launch and target planets permits the computation of the return trajectory. The round-trip trajectory is then obtained by combining the departure and return trajectories.

B. Round-Trip Trajectory Computing Program

Section II-A indicates the inefficiency in the present trajectory design technique. Because of this inefficiency, a round-trip trajectory computing program is being designed. The program will consist of a heliocentric conic program designed in such a way that the departure trajectory and the return trajectory will be patched together, giving a round-trip trajectory rather than two separate one-way trajectories. In addition, the program will be designed so as to minimize the mathematical singularities that arise during the computation of a parabolic or rectilinear trajectory*.

C. Mathematical Limitations

The mathematical limitations in the present heliocentric conic program consist of the following: first, exact parabolic trajectories cannot be computed; second, rectilinear trajectories cannot be computed; and finally, clockwise trajectories* and trajectories having heliocentric central angles* (HCA) greater than 360 deg are not computed. As a result of these limitations, a small portion of data during the decade of 1970 to 1980 is not available. Where missing data are of particular interest, the available data are interpolated, so that the trajectory data are presented only approximately.

*Terms marked with an asterisk are defined in the Nomenclature section.

III. TRAJECTORIES FOR THE 1970-TO-1980 DECADE

The analysis presented in this Report is somewhat different from the analysis usually presented in designing trajectories for missions to the planets. The basic inputs to the heliocentric conic program were launch time and flight time. By choosing these parameters fixed, a unique counterclockwise* solution is obtained as shown in Fig. 2. There is only one heliocentric conic that passes through the two points represented by R_{\oplus} and R_{\odot} and that satisfies the chosen design constraints in Section III-A. Only this type of solution has been computed.

A. Design Constraints

The transfer orbits considered are limited to counterclockwise motion relative to the Sun and to heliocentric central angles of less than 360 deg. Additional constraints are given in Table 1.

B. Degenerate Trajectories — Target Planet in Pseudo-opposition*

Section III-D presents a "theoretical" discussion of the trajectories having launch dates during the decade of 1970 to 1980. The term "theoretical" is emphasized since on some launch dates the one-way trajectories that satisfy the constraints listed in Section III-A are impractical. (The impracticality of these trajectories will be discussed in Section III-D.) These one-way trajectories are known as the degenerate or rectilinear trajectories since the heliocentric phases of these trajectories may be portions of rectilinear ellipses, rectilinear parabolas,

Table 1. Design constraints

Parameters	Constraints
Earth parking orbit radius (initial and final), er^*	1.1000
Mars parking orbit radius, er	0.5916
Launch period	1970 to 1980
Stay time at Mars, days	7
One-way flight times, days	30, 60, 120, and 240

or rectilinear hyperbolas, depending upon the energy of the trajectory. In addition, the rectilinear trajectory may be either a direct trajectory or an indirect trajectory. The direct rectilinear trajectory is defined as a rectilinear trajectory that extends from the launch planet to the target planet without passing through a focus of the conic. This type of trajectory is shown in Fig. 3a for the case of an elliptical departure trajectory. The direct rectilinear trajectory is realistic from the point of view that it is a possible trajectory; however, it is an impractical trajectory. The indirect rectilinear trajectory is defined as a rectilinear trajectory that extends from the launch planet to the target planet but that passes through a focus of the conic as shown in Figs. 3b and 3c for the case of an elliptical departure trajectory. The indirect rectilinear trajectory shown in Fig. 3b passes through the secondary focus, and the indirect rectilinear trajectory shown in Fig. 3c passes through the primary focus, which in this case contains the Sun, i.e., the trajectory passes through the surface of the Sun. The indirect rectilinear trajectory that passes through the secondary focus is also realistic from the point of view that it is a possible trajectory; however, it too is an impractical trajectory. The indirect rectilinear trajectory that passes through the primary focus, i.e., the Sun's surface, is unrealistic as well as impractical. It has theoretical importance only because it completes the overall presentation of data, as will be seen in Section III-D. The degenerate trajectories can occur whenever the target planet is in pseudo-opposition at the same time that the celestial latitude of Mars is zero. This is indeed a rare occasion. However, the nearly degenerate trajectory occurs more frequently, since the inclination of the orbit of Mars is small, about 2 deg, so that the celestial latitude of Mars is near zero at all times. The Earth's celestial latitude is always zero.

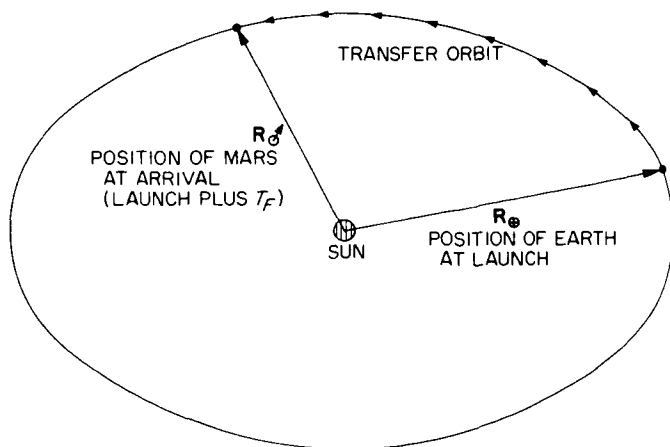


Fig. 2. Heliocentric problem to be solved

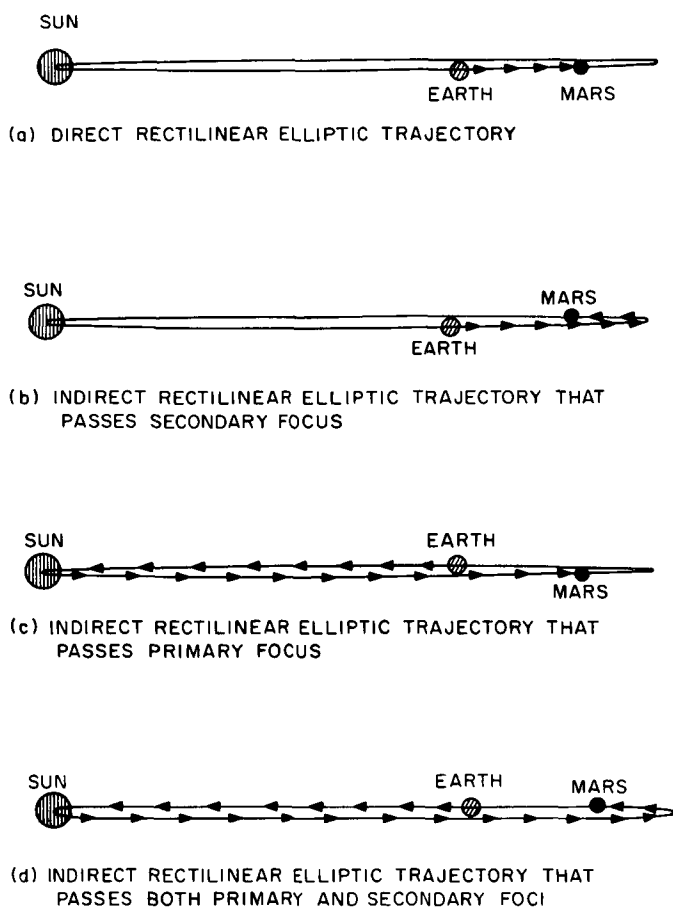


Fig. 3. Difference between direct and indirect rectilinear elliptic trajectories

In the case where the energy is low, i.e., for a long flight time such as 240 days, it is possible to have an indirect, nearly rectilinear elliptic trajectory that passes very near the secondary focus, for one launch day, and an indirect, nearly rectilinear elliptic trajectory that passes very near both the primary focus and the secondary focus, for the next launch day. The first trajectory is shown in Fig. 3b and the second trajectory is shown in Fig. 3d. Both of these trajectories are shown as departure trajectories. The variation described above would occur for two consecutive launch days centered about the day of pseudo-opposition. The energies of these two trajectories, both having the same flight time, are significantly different because of the different paths that are traversed.

Figure 4 is a three-dimensional sketch of the launch planet Earth and the target planet Mars just prior to pseudo-opposition at a time when the celestial latitude

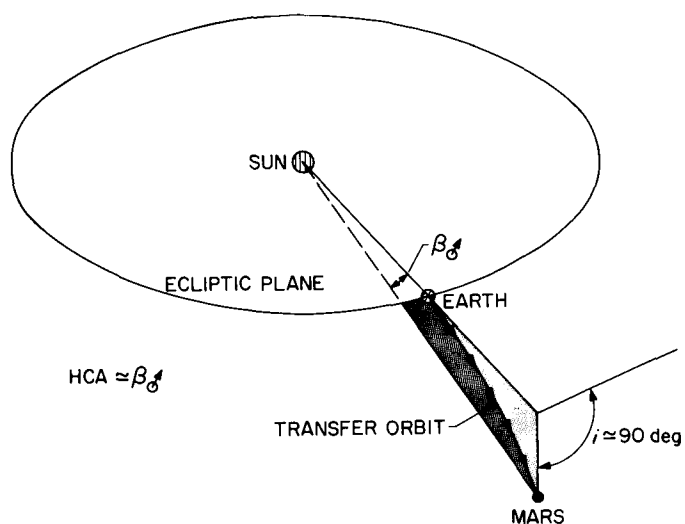


Fig. 4. Direct transfer orbit for planets just prior to pseudo-opposition, $\beta_\delta < 0$

of the target planet is negative. In this case, the departure trajectory is a direct, nearly rectilinear trajectory. The geometric shape of the trajectory depends upon the energy (flight time) under consideration. For a fast trajectory (high energy), the heliocentric phase is a portion of a nearly rectilinear hyperbola or parabola, and for a slow trajectory (low energy), the heliocentric phase is a portion of a nearly rectilinear ellipse. Figure 5 shows the launch planet Earth and the target planet Mars just prior to pseudo-opposition at the time the celestial latitude of the target planet is positive. The geometry relative to the Sun is very similar.

Figure 6 shows the geometry of the two planets relative to the Sun just after pseudo-opposition, so that the

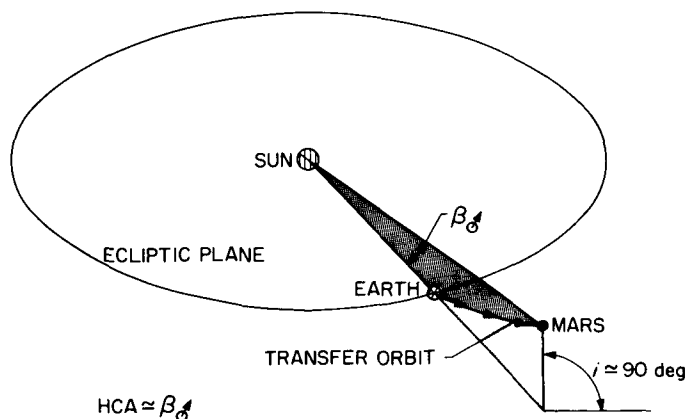


Fig. 5. Direct transfer orbit for planets just prior to pseudo-opposition, $\beta_\delta > 0$

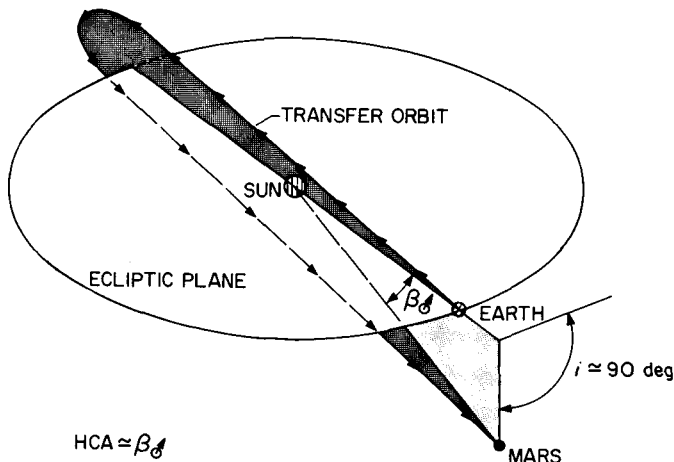


Fig. 6. Indirect transfer orbit for planets just after pseudo-opposition, $\beta_\delta < 0$

departure trajectory is now an indirect, nearly rectilinear trajectory that passes through or very near the Sun's surface. Figures 4 and 6 show the change in the counterclockwise departure trajectory when the target planet passes pseudo-opposition. Both the direct trajectory shown in Fig. 4 and the indirect trajectory shown in Fig. 6, having the same launch day and flight time but differing energy, are possible trajectories when the planets are exactly in pseudo-opposition. However, the indirect trajectory has a much higher energy than the direct trajectory. As a result, as the launch day passes through the day of pseudo-opposition, the departure trajectory changes from a direct trajectory or an indirect trajectory that passes by the secondary focus, depending on the flight time, to an indirect trajectory that passes by the primary focus. As this change in trajectory occurs, the energy jumps to a higher value. The change in the counterclockwise trajectory is a result of the fact that the orbital speed of the Earth is greater than the orbital speed of Mars, so that the Earth catches up to and overtakes Mars in a pseudo fashion (see the Nomenclature for the difference between pseudo-opposition and opposition) relative to the Sun.

The phenomena described in the paragraphs above will appear in the discussion of the characteristics of the computed round-trip trajectories in Section III-D. Note that the discussion above considered the departure trajectory only. Similar phenomena exist for the case of the return trajectory, i.e., the case where Mars is the launch planet and the Earth is the target planet. In this case, the change in the counterclockwise trajectory and energy is opposite to that described above.

C. Out-of-the-Ecliptic Trajectories — Target Planet in Pseudo-conjunction*

Section III-B presented the trajectory problem when the target planet passes through pseudo-opposition. The question of what happens when the target planet passes through pseudo-conjunction now arises. Figures 7 and 8 show the Earth and Mars just before and just after pseudo-conjunction, respectively, at the time the celestial latitude of Mars is positive. The departure trajectories shown are members of a special type of trajectory, namely, the out-of-the-ecliptic trajectory. This type of trajectory is characterized by an inclination relative to the ecliptic plane of approximately 90 deg and an HCA of approximately 180 deg. In addition, the energy required for this out-of-the-ecliptic trajectory is higher than the trajectories before and after the occurrence of this trajectory. The before-and-after trajectories are nearly in the ecliptic plane, since the inclination of the orbit of Mars is small. The reason for this phenomenon can best be explained by referring to the vector diagrams shown in Figs. 7, 8, and 9. Note that since the hyperbolic excess speed with respect to the Earth, $(V_\infty)_{\oplus 1}$, is a measure of the additional energy required for a departure trajectory, the variation of energy required with respect to inclination is obtained by observing the variation of the vector $(V_\infty)_{\oplus 1}$ with respect to inclination. The vector diagrams in Fig. 9 show that $(V_\infty)_{\oplus 1}$ is maximum for an out-of-the-ecliptic trajectory and minimum for an in-the-ecliptic trajectory for any fixed heliocentric inertial speed $(V_1)_{\oplus 0}$ at injection into the heliocentric conic. Clearly, since the magnitude of $(V_1)_{\oplus 0}$ for a fixed flight time and the vector V_\oplus do not change significantly over a period of several launch

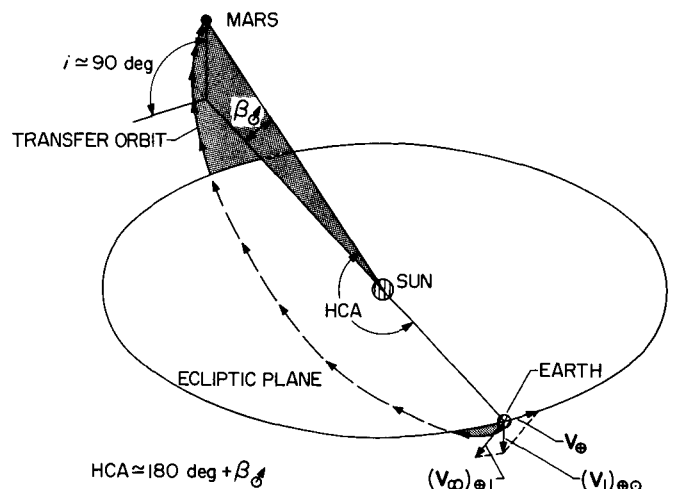


Fig. 7. Out-of-the-ecliptic transfer orbit for planets just prior to pseudo-conjunction, $\beta_\delta > 0$

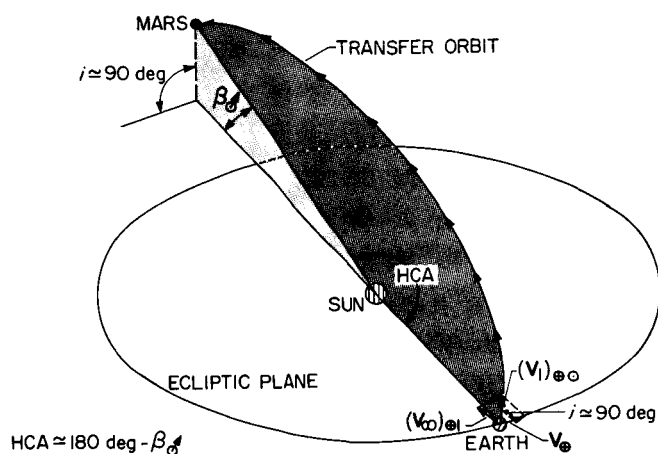


Fig. 8. Out-of-the-ecliptic transfer orbit for planets just after pseudo-conjunction, $\beta_\delta > 0$

days centered about pseudo-conjunction, the change of $(V_\infty)_{\oplus}$ is due primarily to the change in the direction of $(V_1)_{\oplus}$, i.e., inclination of the trajectory plane. This implies that as the inclination varies from near 0 deg to 90 deg and back to near 0 deg, the speed $(V_\infty)_{\oplus}$ varies from a low value to a high value and back to a low value. As a result, as the target planet changes from positions prior to pseudo-conjunction to positions after pseudo-conjunction, the counterclockwise departure trajectory should vary from a trajectory having an inclination near 0 deg and of the type shown in Fig. 7, through a pair of trajectories having inclinations of 90 deg, to a trajectory having an inclination near 0 deg and of the type shown in Fig. 8. As this occurs, a plot of the speed $(V_\infty)_{\oplus}$ vs launch date should show a peak. Note that if a launching occurs exactly at the time of pseudo-conjunction, then both of the types of departure trajectory shown in Figs. 7 and 8 (the pair having inclinations of 90 deg) are possible, each having the same flight time but different energies. The type of trajectory shown in Fig. 7, with an HCA > 180 deg, will have the greater energy since a greater distance must be traveled in the same time of flight. Again, the geometric shape

of the trajectory depends upon the flight time (energy) under consideration. For a fast trajectory (high energy), the heliocentric phase is a portion of a hyperbola or parabola and for a slow trajectory (low energy), the heliocentric phase is a portion of an ellipse.

The out-of-the-ecliptic trajectory having an inclination of exactly 90 deg and an HCA of nearly 180 deg is not similar to the Hohmann transfer orbit*, which requires minimum $(V_\infty)_{\oplus}$. The Hohmann transfer orbit has an HCA of exactly 180 deg, a circumstance that requires the celestial latitude of Mars to be zero at the time of pseudo-conjunction, thus forcing the inclination of the transfer orbit to be 0 deg. This, of course, is a rare occurrence. As a result, even though the inclination of the orbit plane of Mars to the ecliptic plane is only about 2 deg, it is a very important 2 deg, since this causes the celestial latitude to be primarily non-zero at pseudo-conjunction. This phenomenon indicates the importance of a three-dimensional conic analysis.

The phenomena described in the paragraphs above will appear in the next Section during the discussion of the characteristics of the counterclockwise round-trip trajectories. Note that the discussion above considered the departure trajectory only. Similar phenomena exist for the case of the return trajectory.

D. Theoretical Discussion

The characteristics of round-trip planetary trajectories are similar in many respects to one-way interplanetary trajectories. The similarity may be seen by considering the Keplerian-orbit approximations to the round-trip and one-way trajectories. From this viewpoint the round-trip trajectory consists primarily of two one-way trajectories, one leaving the initial launch planet and one returning to the initial launch planet. As a result, the characteristics of the round-trip trajectory are just the characteristics of the two one-way trajectories properly combined.

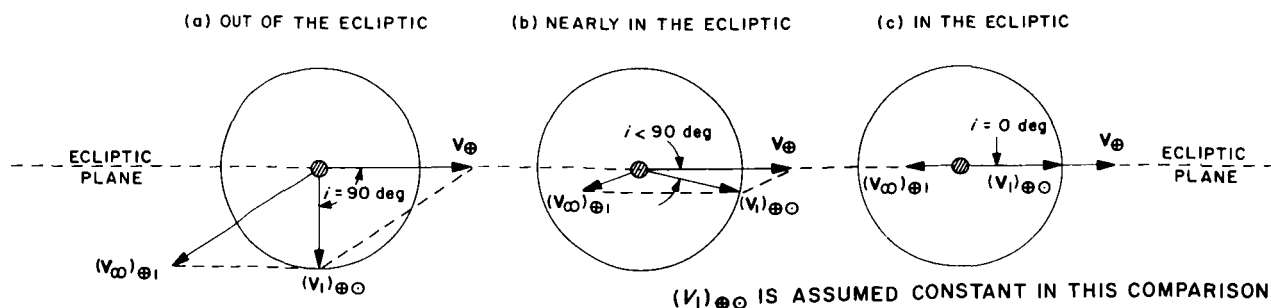


Fig. 9. Dependence of the hyperbolic excess speed on the inclination of the transfer orbit

The design of a round-trip trajectory differs from the design of a one-way trajectory in that the optimization procedure, from the viewpoint of energy required, requires choosing the proper combination of the two one-way trajectories that are not necessarily optimum from the viewpoint of one-way transit but that do combine to give the optimum round-trip characteristics. This implies that the notable work appearing in Refs. 1 and 2 is of little help in designing round-trip trajectories.

The characteristics of the high-energy trajectories from Earth to Mars and return for the entire decade beginning January 1970 and ending January 1980 have been investigated for the four round-trip flight times of 67, 127, 247, and 487 days. The round-trip flight time consists of the sum of the departure flight time, the stay time at the target planet, and the return flight time. In this analysis, the departure flight time is the same as the return flight time. As a result, the round-trip flight times of 67, 127, 247, and 487 days correspond to the one-way flight times of 30, 60, 120, and 240 days, respectively, associated with either the departure or return trajectories, and a stay time of 7 days in the orbit about Mars. The trajectories were computed once for each day (0 hr GMT) in the decade 1970 to 1980, using the trajectory design technique described in Section II-A, listed in tabular form, bound in book form according to year, and placed in the trajectory library at the Jet Propulsion Laboratory. This Report presents only the energy characteristics of these trajectories in graphical form in order to show the scope of the analysis and indicate the optimum launch periods, from the viewpoint of energy required, during the decade 1970 to 1980. Detailed trajectory data similar to those of Ref. 1 are not presented here, but may be obtained from the Jet Propulsion Laboratory.

Two parameters are used in this Report to indicate the energy required to accomplish the previously prescribed mission on a given launch date. The first parameter is the total hyperbolic excess speed, $(V_\infty)_T$, which consists of the sum of the hyperbolic excess speeds required for leaving the vicinity of the Earth, arriving at the vicinity of Mars, leaving the vicinity of Mars, and arriving at the vicinity of the Earth. (The hyperbolic excess speeds upon arriving at the two planets must be added in to form $(V_\infty)_T$ for the previously prescribed mission, since these speeds are a measure of the energy that must be removed from the energy of each transfer orbit in order to obtain the corresponding parking orbit.) The second parameter is the total speed increment required, $(\Delta V)_T$, which consists of the sum of the speed increments required in leaving the parking orbit about the Earth,

entering the parking orbit about Mars, leaving the parking orbit about Mars, and reentering the parking orbit about the Earth. The speed increment $(\Delta V)_T$ clearly represents the energy required for the given mission but, unfortunately, $(\Delta V)_T$ depends upon the parking orbits about the two planets. It would be more advantageous if a parameter independent of the parking orbits could be used to represent the energy required. Such a parameter is $(V_\infty)_T$, which is independent of the two parking orbits for the conic analysis used in this Report.

Appendix A shows that $(\Delta V)_T$ can be related to $(V_\infty)_T$ so that $(V_\infty)_T$ can be used to represent the energy required for the given mission, using pairs of parking orbits other than those used in this Report (Eq. A-8). For all reasonable pairs of parking orbits about the planets, the relation between $(\Delta V)_T$ and $(V_\infty)_T$ simplifies to Eq. (A-13), $(\Delta V)_T = (V_\infty)_T - 2 [(V_c)_\oplus + (V_c)_\delta]$, for a sufficiently fast flight time. In addition, Eq. (A-16) shows that $(\Delta V)_T = 0.828 [(V_c)_\oplus + (V_c)_\delta]$ for the case where $(V_\infty)_T = 0$ for all pairs of parking orbits about the planets. From these facts and from the actual and approximate plots of $(\Delta V)_T$ vs $(V_\infty)_T$ shown in Fig. 10 for the pair of parking orbits chosen in this Report, the plot of $(\Delta V)_T$ vs $(V_\infty)_T$ may be constructed to good accuracy for all reasonable pairs of parking orbits about the planets. In this manner,

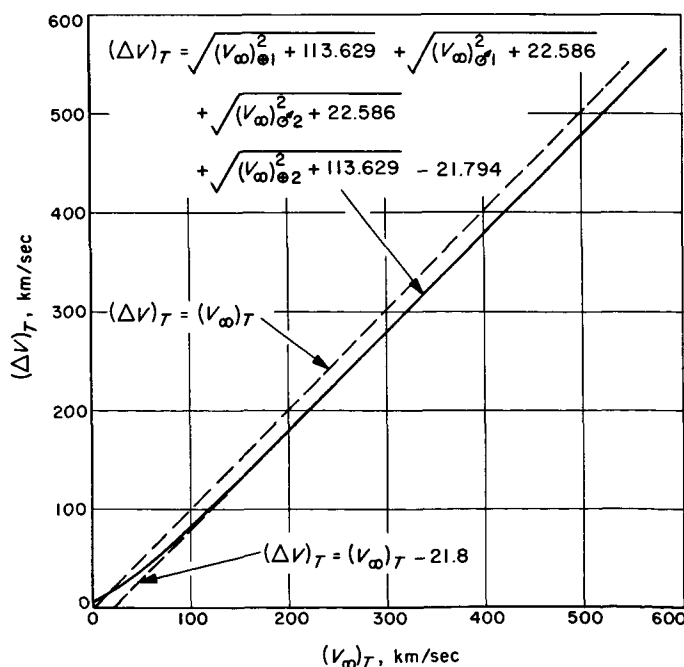


Fig. 10. Total speed increment from Earth orbit to Mars orbit to Earth orbit vs the sum of geocentric and areocentric hyperbolic excess speeds

$(\Delta V)_T$ can be obtained directly from $(V_\infty)_T$. As a result, the plots of $(V_\infty)_T$ vs launch date from the Earth appearing in Figs. B-1 through B-11 in Appendix B are discussed in detail in the following pages. This discussion holds not only for the particular pair of parking orbits chosen in this analysis but for all reasonable pairs of parking orbits. For convenience, plots of $(\Delta V)_T$ vs launch date from the Earth are presented in Figs. B-12 through B-21 for the particular pair of parking orbits chosen in this analysis.

In order to indicate the variation of the energy requirements for the round-trip trajectories with launch date and flight time over a large interval of time, a decade plot of $(V_\infty)_T$ vs launch date from the Earth is presented in Fig. B-1 for each of the four round-trip flight times specified previously. Flight time is chosen as the parameter in this and similar figures because, for manned space flights to Mars, sufficient life support equipment and supplies will be provided for a specific length of time, which will dictate a maximum allowable flight time. As a result, the flight time herein is actually the maximum allowable flight time for the mission. Each of the four curves appearing in Fig. B-1 is labeled according to the one-way flight time rather than the round-trip flight time. For example, the upper curve is designated 30 days and should be interpreted as the curve representing $(V_\infty)_T$ vs launch date from the Earth for a departure flight time of 30 days, a stay time of 7 days, and a return flight time of 30 days. This procedure is used throughout Figs. B-1 through B-21.

Each of the curves in Fig. B-1 exhibits a basic periodic behavior if the period of variation is considered as the interval of time between two adjacent crests of the curve. However, the periodicity is not exact, owing to the changing Earth-Sun-Mars geometry during the decade.

Within each period, there is a launch date that requires a relative minimum $(V_\infty)_T$ and a launch date that requires a relative maximum $(V_\infty)_T$. These relative extrema do not necessarily occur on the same launch dates as the relative extrema for the corresponding one-way interplanetary trajectory (departure trajectory). Table 2 presents the relative minimum $(V_\infty)_T$ and the corresponding launch date from the Earth in each period of each of the four flight time curves.

Consider the 30-day curve. The first period is approximately from August 1, 1970, to August 1, 1972, a length of 2 years as shown. The remaining periods are approximately 2 years in length if the portion of the curve in 1979 is considered as two crests rather than one crest. Note that only part of the fifth period appears in this decade plot, since the periods are not symmetrically spaced during the decade (see Appendix C, Table C-1). As the decade is traversed from earlier to later dates, the crests become flatter and the relative maximum $(V_\infty)_T$ of the crests diminishes. On the other hand, as the decade is traversed from earlier to later dates, the troughs become narrower and the relative minimum $(V_\infty)_T$ of the troughs rises. During each period, the curve exhibits two finite discontinuities indicated by vertical dashed lines, one on each side of the minimum $(V_\infty)_T$ of the trough, and two peaks situated on the crest. The causes of these discontinuities are discussed later in this Report, along with the causes of the small peaks occurring on the crests. Note that the peaks on the crests occur later in each consecutive period.

Consider the 60-day curve. This curve is analogous to the 30-day curve having a first period approximately from July 1, 1970, to July 1, 1972, also a length of 2 years. The 60-day curve is flatter than the 30-day curve in its entirety and has larger peaks occurring on the crests.

Table 2. Relative minimum $(V_\infty)_T$ for the decade 1970 to 1980

Period	One way $T_F = 30$ days		One way $T_F = 60$ days		One way $T_F = 120$ days		One way $T_F = 240$ days	
	Launch date from Earth	$(V_\infty)_T$, km/sec	Launch date from Earth	$(V_\infty)_T$, km/sec	Launch date from Earth	$(V_\infty)_T$, km/sec	Launch date from Earth	$(V_\infty)_T$, km/sec
1	Jul 11, '71	91.276	Jun 9, '71	50.868	Apr 22, '71	34.891	Jan 1, '71	24.676
2	Sep 12, '73	105.788	Aug 7, '73	58.682	May 7, '73	37.322	Dec 3, '72	24.560
3	Nov 6, '75	137.389	Sep 27, '75	76.201	Jun 21, '75	46.467	Dec 31, '74	26.950
4	Dec 18, '77	158.458	Nov 16, '77	87.595	Aug 4, '77	55.131	Jan 10, '77	31.834
5	Jan 24, '80	164.017	Dec 27, '79	90.492	Dec 7, '79	58.415	Sep 18, '79	35.023

In addition, the difference between the maximum $(V_{\infty})_T$ and the minimum $(V_{\infty})_T$ in any one period is smaller for the 60-day curve than for the 30-day curve. Similarly, the discontinuities are smaller.

Consider the 120-day curve. The variation of this curve is similar to the 60-day curve having a first period approximately from March 1, 1970, to May 1, 1972, a length of 2 years and 2 months. The 120-day curve has a different appearance from the 30- or 60-day curve, in that the crests have become completely flattened and appear more as plateaus than crests. The two peaks are still present, but now they occur in the troughs rather than on the plateaus. Furthermore, the two peaks occur in the same relative location in each period. As the decade is traversed from earlier to later dates, the plateaus become distorted, and the relative maximum $(V_{\infty})_T$ of the plateaus diminishes. The plateaus distort more and more toward two pointed crests similar to the formation of the two crests for the 30- and 60-day curves in 1979. On the other hand, as the decade is traversed from earlier to later dates, the troughs become narrower and the relative minimum $(V_{\infty})_T$ of the troughs rises. Note that the 120-day curve is continuous, i.e., there are no visible discontinuities as in the 30- and 60-day curves. Also, note that the small peaks are attenuated as the flight time is increased, i.e., the small peaks of the 120-day curve are larger than those of the 60-day curve. Finally, the difference between the maximum $(V_{\infty})_T$ and the minimum $(V_{\infty})_T$ in any one period is smaller for the 120-day curve than for the 60-day curve.

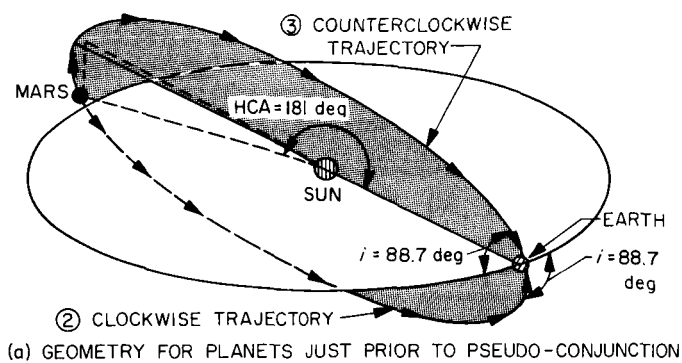
Consider the 240-day curve. The variation of this curve is analogous to that of the 120-day curve having a first period approximately from October 1, 1969, to January 1, 1972, a length of 2 years and 2 months. The attenuations described for the 120-day curve are more pronounced for the 240-day curve. Again, the 240-day curve has two small peaks occurring in each of the periods and no discontinuities, just as in the case of the 120-day curve.

Figure B-1 and Table 2 show that the absolute minimum $(V_{\infty})_T$ for the 30-, 60-, and 120-day curves in the decade 1970 to 1980 occur during the first period, and the absolute minimum $(V_{\infty})_T$ for the 240-day curve occurs during the second period. In addition, the periodic behavior of the four curves shown implies that later decades should have similar appearances so that approximate extrapolations can be made if necessary. A word of caution is advisable at this point of the discussion. Owing to the nature of the curves in Figs. B-1

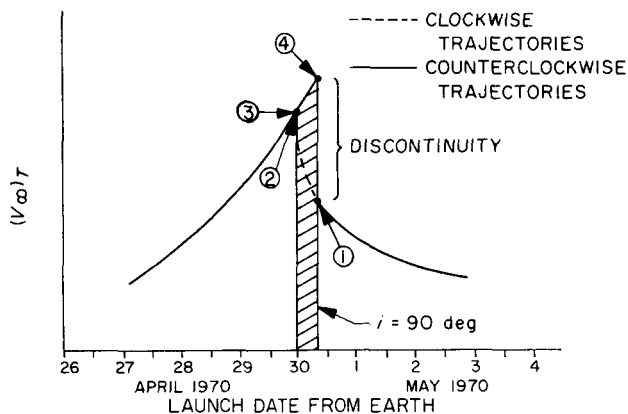
through B-21, interpolation between the flight times presented is not advisable. The limited amount of data does not permit the determination of the launch dates from the Earth on which the peaks and discontinuities occur for other flight times.

The previous discussion indicates the peculiar variations which arise in the design of round-trip planetary trajectories but which usually do not appear in the design of one-way interplanetary trajectories: namely, the small peaks and discontinuities. The causes of these peculiar variations are best explained with the use of the detailed plots of $(V_{\infty})_T$ vs launch date from the Earth appearing in Figs. B-2 through B-11. These plots are centered about the relative minimum or maximum $(V_{\infty})_T$, so that some of the round-trip trajectory data in Fig. B-1 are not shown in detail.

Figure B-2 presents plots of $(V_{\infty})_T$ vs launch date from the Earth for the year of 1970. Consider the 30-day curve. For the launch date of January 1, 1970, the heliocentric Keplerian approximation to the round-trip planetary trajectory consists of (1) a hyperbolic departure trajectory having an eccentricity of 1.15, an inclination* of 0.4 deg, and an HCA of 298 deg, and (2) a hyperbolic return trajectory having an eccentricity of 10.21, an inclination of 0.3 deg, and an HCA of 126 deg. Since both one-way trajectories are hyperbolic, $(V_{\infty})_T$ is rather large. The 30-day curve in Fig. B-2 shows that $(V_{\infty})_T$ is approximately 484 km/sec. For the following launch dates, $(V_{\infty})_T$ increases steadily until April 30, where a small peak appears. From the books of trajectories in the JPL trajectory library, the heliocentric Keplerian approximation to the round-trip planetary trajectory for the launch date of April 30 consists of (1) a hyperbolic departure trajectory having an eccentricity of 1.80, an inclination of 1.6 deg, and an HCA of 240 deg, and (2) a hyperbolic return trajectory having an eccentricity of 5.21, an inclination of 88.7 deg, and an HCA of 181 deg. The departure trajectory is of the type considered for high-energy one-way interplanetary missions, but the return trajectory is of a special type not usually considered for high-energy one-way interplanetary missions because of the relatively higher energy required. This return trajectory is the counterclockwise return trajectory shown in Fig. 11a. The inclination of this special type of trajectory is very near 90 deg, i.e., it is an out-of-the-ecliptic trajectory requiring higher energy than trajectories that are in or nearly in the ecliptic plane as discussed in Section III-C. The small peak appearing on the 30-day curve in Fig. B-2 is attributed to the variation of the inclination of the return



(a) GEOMETRY FOR PLANETS JUST PRIOR TO PSEUDO-CONJUNCTION



(b) A PORTION OF THE 30-day CURVE IN FIG. B-2, CENTERED ABOUT PSEUDO-CONJUNCTION

Fig. 11. Dependence of the hyperbolic excess speed on the direction of the transfer orbit for pseudo-conjunction

trajectory from near 0 deg to 90 deg to near 0 deg over the several launch days centered about April 30, pseudo-conjunction.

Fig. 11b shows a detailed portion of the 30-day curve in Fig. B-2, as well as a rather interesting result. The Figure shows that when the data were interpolated between days to obtain the peak in Fig. B-2 (recall that trajectories were computed at one-day intervals), trajectory data for round-trip trajectories having clockwise return trajectories were presented. If data for round-trip trajectories having only counterclockwise return trajectories were presented, the curve would not show a peak but would show a small discontinuity as indicated by the solid lines in Fig. 11b. The discontinuity would occur at the launch time where the inclination of the return trajectory is 90 deg. At this launch time there would be two possible solutions (the pair of round-trip trajectories having return trajectories with inclinations of 90 deg) indicated by numbers ① and ④ in Fig. 11b, as was discussed in

Section III-C. However, the interesting result from Figs. 11a and 11b is that at a particular launch time very near 0 hr GMT on April 30, the counterclockwise and clockwise return trajectories, indicated by the numbers ② and ③, exhibit the same $[(V_{\infty})_{\oplus 2} + (V_{\infty})_{\oplus 2}]$, i.e., the same $(V_{\infty})_T$, since the departure trajectory is the same for both cases. This point of the curve is the double point* of the peak shown in Fig. B-2. The interpretation of this result is as follows: there is a trade-off between the added energy required to travel the greater distance for the counterclockwise trajectory and the added energy required to compensate for the loss of the effective orbital energy of the launch planet for the clockwise trajectory. This trade-off, as well as the occurrence of the discontinuity, will be discussed in greater detail later in this Section when the case of pseudo-opposition is considered. Figure 11b also shows that there are times when the round-trip trajectory having a clockwise return trajectory has lower $(V_{\infty})_T$ than the round-trip trajectory having a counterclockwise return trajectory as shown in the cross-hatched area. Finally, note that if the inclination of the orbit plane of Mars is neglected, i.e., if a two-dimensional conic analysis is made, the peak appearing on the 30-day curve in Fig. B-2 will not appear.

Immediately after these launch days, $(V_{\infty})_T$ continues to increase slightly and then decreases slightly until August 28, where a second small peak appears. From the JPL trajectory books, the heliocentric Keplerian approximation to the round-trip planetary trajectory for the launch date of August 28 consists of (1) a hyperbolic departure trajectory having an eccentricity of 5.79, an inclination of 87.1 deg, and an HCA of 178 deg, and (2) a hyperbolic return trajectory having an eccentricity of 1.77, an inclination of 2.0 deg, and an HCA of 243 deg. In this case the departure trajectory is an out-of-the-ecliptic trajectory of the type shown in Fig. 8, and the return trajectory is of the type considered for high-energy one-way interplanetary missions. The second small peak appearing on the 30-day curve in Fig. B-2 is attributed to the variation of the inclination of the departure trajectory from near 0 deg to 90 deg to near 0 deg over the several launch days centered about August 28, pseudo-conjunction. Furthermore, this peak presents some round-trip trajectory data where the departure trajectory is clockwise. Note that pseudo-conjunction can occur more than once in a period—once for the departure trajectory and once for the return trajectory for a given flight time—whereas conjunction* can occur just once in any period of the curves for the planet Mars. Immediately after these launch days, $(V_{\infty})_T$ continues to decrease slightly without further irregularities in Fig. B-2.

Consider the 60-day curve in Fig. B-2. For the launch date of January 1, 1970, the heliocentric Keplerian approximation to the round-trip planetary trajectory consists of (1) a hyperbolic departure trajectory having an eccentricity of 1.04, an inclination of 0.2, and an HCA of 314 deg and (2) a hyperbolic return trajectory having an eccentricity of 2.5, an inclination of 1.5, and an HCA of 168 deg. Again, since both one-way trajectories are hyperbolic, $(V_\infty)_T$ is large. The 60-day curve in Fig. B-2 shows that $(V_\infty)_T$ is approximately 240 km/sec. For the following launch dates, $(V_\infty)_T$ increases slightly until January 28, 1970, where a small peak appears. From the JPL trajectory books, the heliocentric Keplerian approximation to the round-trip planetary trajectory for the launch date of January 28 consists of (1) a hyperbolic departure trajectory having an eccentricity of 1.08, an inclination 0.7 deg, and an HCA of 302 deg, and (2) a hyperbolic return trajectory having an eccentricity of 2.33, an inclination of 83.7 deg, and an HCA of 181 deg. The departure trajectory is of the type considered for high-energy one-way interplanetary missions, but the return trajectory is an out-of-the-ecliptic trajectory. The first small peak appearing on the 60-day curve in Fig. B-2 is attributed to the variation of the inclination of the return trajectory from near 0 deg to 90 deg to near 0 deg over the several launch days centered about January 28, 1970, pseudo-conjunction. As in the case of the 30-day curve, the small peak presents some round-trip trajectory data where the return trajectory is clockwise.

Immediately after these launch days, $(V_\infty)_T$ continues to increase slightly and then decreases slightly until September 22, where a second small peak appears. From the JPL trajectory books, the heliocentric Keplerian approximation to the round-trip planetary trajectory for the launch date of September 22 consists of (1) a hyperbolic departure trajectory having an eccentricity of 2.55, an inclination of 80.0 deg, and an HCA of 178 deg and (2) a hyperbolic return trajectory having an eccentricity of 1.08, an inclination of 1.7 deg, and an HCA of 305 deg. In this case the departure trajectory is an out-of-the-ecliptic trajectory and the return trajectory is of the type considered for high-energy one-way interplanetary missions. The second small peak appearing on the 60-day curve in Fig. B-2 is attributed to the variation of the inclination of the departure trajectory from near 0 deg to 90 deg to near 0 deg over the several launch days centered about September 22, pseudo-conjunction. Furthermore, this peak presents some round-trip trajectory data where the departure trajectory is clockwise.

Immediately after these launch days, $(V_\infty)_T$ continues to decrease slightly until the date of January 6, 1971, where a discontinuity appears and $(V_\infty)_T$ becomes double-valued. Investigation of the heliocentric angles, eccentricities, inclinations, and the celestial latitudes and longitudes of the launch and target planets on and around January 6 show that the two solutions possible on January 6 have near-degenerate return trajectories.

The upper portion of the 60-day curve in Fig. B-2 represents round-trip trajectories having hyperbolic departure and return trajectories. As this curve is traversed from earlier to later dates, the eccentricity of the departure trajectory becomes larger, whereas the eccentricity of the return trajectory becomes smaller, i.e., it approaches one. At the same time the launch and target planets for the return trajectory approach pseudo-opposition* (this term should not be confused with pseudo-conjunction) so that the return geometry for the launch date of January 6, 1971, requires the near-degenerate trajectory (see Section III-B). As a result, the upper branch of the 60-day curve approaches a value of $(V_\infty)_T$ that represents a hyperbolic departure trajectory and a near-degenerate return trajectory that is an indirect, nearly rectilinear hyperbolic trajectory passing very near the primary focus containing the Sun. This limiting case is the higher-energy solution for the launch date of January 6.

The second solution for the launch date of January 6, 1971, is similar to the first solution, with the exception that the near-degenerate return trajectory is a direct, nearly rectilinear elliptic trajectory and is therefore of a lower energy, since less distance is traveled in the one-way flight time of 60 days. Figures 3a and 3c show the difference between the direct and indirect trajectories for the case of elliptical departure trajectories (see Section III-B). At this point the data seem questionable. Why should this discontinuity appear in a curve of energy vs launch date when all motions in the Universe are continuous? The answer lies in the design constraints chosen for this analysis. This analysis and Report are concerned with the computation of counterclockwise one-way trajectories only, i.e., trajectories that encircle the Sun in the same direction as the Earth's orbit (the clockwise one-way trajectories that appeared earlier resulted from the interpolations of the data and not from computations made).

Figure 2 shows the counterclockwise one-way trajectory for the case of a departure trajectory. It is also possible to compute a clockwise one-way trajectory that has the same launch day and flight time as the counterclockwise

one-way trajectory, i.e., there are two one-way trajectories for any given launch day and flight time combination if clockwise trajectories are considered. However, the clockwise one-way trajectory usually requires a higher energy. Consider the direction of the two possible trajectories when the inclination is exactly 90 deg. Figures 4 and 6 show departure trajectories similar to this pair of trajectories if the flight times of the departure trajectories are assumed to be the same. Clearly the direction of the trajectories cannot be compared to the direction of the Earth's orbit on which the definition of clockwise and counterclockwise relies, so that these terms do not pertain to this situation. As a result, the present computations supply data for both one-way trajectories whenever the geometry of the problem is such that the inclination of the one-way trajectory plane to the ecliptic is 90 deg. This, of course, can occur only at pseudo-conjunction or pseudo-opposition.

During the previous discussion of the peaks appearing at pseudo-conjunction, it was pointed out that if data for round-trip trajectories having only counterclockwise one-way trajectories were presented, discontinuities would appear in place of the peaks. The reason that data for these discontinuities were available is now clear. On January 6, the Earth is in pseudo-opposition for the return trajectory and so has two solutions. The lower branch of the 60-day curve then begins on January 6 with a $(V_\infty)_T$ of 161 km/sec, which represents a hyperbolic departure trajectory with a direct, nearly rectilinear elliptic return trajectory and continues with decreasing $(V_\infty)_T$. The values for $(V_\infty)_T$ to the right of the discontinuity represent counterclockwise hyperbolic departure trajectories and counterclockwise elliptic return trajectories. As a result, the discontinuity is a consequence of the change in the type of return trajectory. The constraint that only counterclockwise trajectories are to be computed forces the return trajectory to be an indirect, nearly rectilinear hyperbolic trajectory just prior to pseudo-opposition and a direct, nearly rectilinear elliptic trajectory just after pseudo-opposition, as shown in Fig. 12a.

By including clockwise one-way trajectories in this analysis, direct, nearly rectilinear elliptic trajectories prior to pseudo-opposition may be obtained as shown in Fig. 12a. In this way a continuous plot of $(V_\infty)_T$ vs launch date may be obtained for the 60-day flight time in Fig. B-2, similar to that in Fig. 12b. Figures 12a and 12b show that the clockwise elliptic return trajectories prior to pseudo-opposition require less added energy or $(V_2)\sigma_0$ than the counterclockwise hyperbolic return trajectories and that,

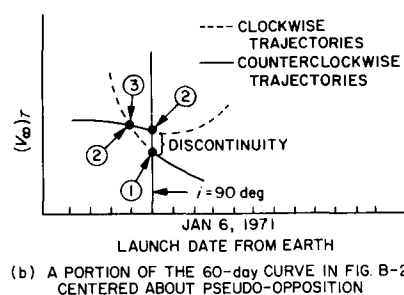
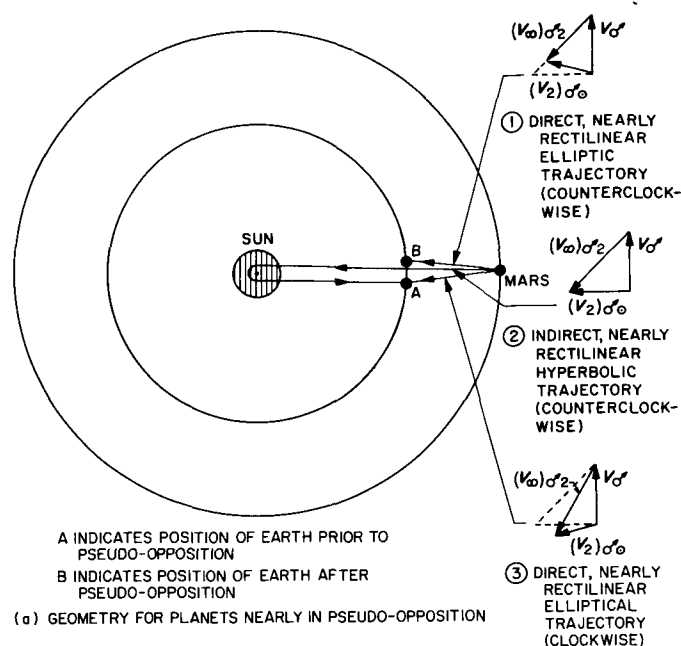


Fig. 12. Dependence of the hyperbolic excess speed on the direction of the transfer orbit for pseudo-opposition

in the case of return trajectories with inclinations of nearly 90 deg, there is a trade-off between the added energy required to travel the greater distance for the counterclockwise trajectory and the added energy required to compensate for the loss of the effective orbital energy of the launch planet for the clockwise trajectory. As a result, clockwise trajectories must be computed in this and similar regions in order to present all the minimum energy cases throughout the decade.

Figure 12b shows several points of the 60-day curve in Fig. B-2 labeled by numbers that represent the type of return trajectories listed in Fig. 12a. Note that if the data for the round-trip trajectories having clockwise return trajectories are added to the 60-day curve in Fig. B-2 for the dates just prior to pseudo-opposition on January 6, 1971, a continuous curve is obtained, but that at one point of this curve, a double point exists as in the case of pseudo-conjunction. The double point represents the

launch date from the Earth on which the return trajectories designated by ② and ③ are the two possible return trajectories for this launch date and flight time combination. Furthermore, the two round-trip trajectories having these particular return trajectories require the same energy or $(V_{\infty})_T$ even though the counterclockwise return trajectory has a larger distance traveled that is associated with it. The remaining portion of the 60-day curve is without peculiarities.

Consider the 120-day curve in Fig. B-2. For the launch date of January 1, 1970, the heliocentric Keplerian approximation to the round-trip planetary trajectory consists of (1) an elliptic departure trajectory having an eccentricity of 0.98, an inclination of 4.5, and an HCA of 346 deg, and (2) an elliptic return trajectory having an eccentricity of 0.87, an inclination of 1.3, and an HCA of 252 deg. Since both one-way trajectories are elliptic, $(V_{\infty})_T$ is considerably less for the 120-day curve than for the 60-day curve. Figure B-2 shows that $(V_{\infty})_T$ is approximately 118 km/sec. For the following dates, $(V_{\infty})_T$ remains approximately the same, first decreasing slightly and then increasing slightly until the launch date of July 14, where $(V_{\infty})_T$ begins decreasing rapidly. An investigation of the detailed trajectory printout about this launch date reveals that the return trajectory for the launch date of July 14 is an indirect, nearly rectilinear elliptic trajectory that passes very near the primary focus containing the Sun, and the return trajectory for the launch date of July 15 is a direct, nearly rectilinear elliptic trajectory, so that pseudo-opposition and a double point occur at some time on July 14 or 15 (July 14 is arbitrarily chosen until more detailed data are obtained).

It is interesting to note that the discontinuity caused by the change of the return trajectory from indirect to direct, as in the case of the 60-day curve, is so small that it does not appear in the case of the 120-day curve in Fig. B-2; however, it does exist. In fact, Fig. 12b is very similar to the portion of the 120-day curve in Fig. B-2 centered about July 14. The occurrence of the double point implies that during the interpolation of the curve from July 14 to July 15, data for round-trip trajectories having clockwise return trajectories have been represented. However, the amount of data represented is small. As before, the decrease in $(V_{\infty})_T$ exhibited from July 14 to July 15 is attributed to the lower energy required to traverse a shorter distance than to traverse a longer distance in a fixed flight time.

The value for $(V_{\infty})_T$ continues to decrease until November 14, where a small peak appears. From the JPL tra-

jectory books, the heliocentric Keplerian approximation to the round-trip planetary trajectory for the launch date of November 14 consists of (1) an elliptic departure trajectory having an eccentricity of 0.88, an inclination of 17.6 deg, and an HCA of 180 deg, and (2) an elliptic return trajectory having an eccentricity of 0.47, an inclination of 0.2 deg, and an HCA of 61 deg. The departure trajectory is practically an out-of-the-ecliptic trajectory, and the return trajectory is of the type considered for high-energy, one-way interplanetary missions. The small peak appearing on the 120-day curve in Fig. B-2 is attributed to the variation of the inclination of the departure trajectory from near 0 deg to 90 deg to near 0 deg over the several launch days centered about November 14, pseudo-conjunction. As in the 30- and 60-day curves, the peak presents some round-trip trajectory data where the departure trajectory is clockwise. Immediately following these launch dates, $(V_{\infty})_T$ continues to decrease slightly without further irregularities in Fig. B-2.

Consider the 240-day curve in Fig. B-2. For the launch date of January 1, 1970, the heliocentric Keplerian approximation to the round-trip planetary trajectory consists of (1) an elliptic departure trajectory having an eccentricity of 0.88, an inclination of 2.8, and an HCA of 41 deg and (2) an elliptic return trajectory having an eccentricity of 0.64, an inclination of 1.89, and an HCA of 77 deg. The 240-day curve in Fig. B-2 shows that $(V_{\infty})_T$ is approximately 81 km/sec. For the following dates, $(V_{\infty})_T$ remains approximately the same, increasing slightly until the launch date of March 14, where $(V_{\infty})_T$ begins decreasing rapidly. An investigation of the detailed trajectory printout about this launch date reveals that the departure trajectory for the launch date of March 14 is an indirect, nearly rectilinear elliptic trajectory passing by the secondary focus and that the departure trajectory for the launch date of March 15 is an indirect, nearly rectilinear elliptic trajectory of lower energy that passes very near both the primary focus containing the Sun and the secondary focus (see Section III-B), so that a double point occurs at some time on March 14. As a result, $(V_{\infty})_T$ decreases from March 14 to March 15 as in the case of the double point occurring for the 120-day curve. Furthermore, data for round-trip trajectories having clockwise departure trajectories are presented.

The value for $(V_{\infty})_T$ continues to decrease until July 21, where a peak appears. From the JPL trajectory books, the heliocentric Keplerian approximation to the round-trip planetary trajectory for the launch date of July 21 consists of (1) an elliptic departure trajectory having an eccentricity of 0.51, an inclination of 0.1 deg, and an HCA of

296 deg and (2) an elliptic return trajectory having an eccentricity of 0.2, an inclination of 78.8 deg, and an HCA of 180 deg. The departure trajectory is of the type considered for high-energy one-way interplanetary missions and the return trajectory is an out-of-the-ecliptic trajectory. The peak appearing on the 240-day curve in Fig. B-2 is attributed to the variation of the inclination of the return trajectory from near 0 deg to 90 deg to near 0 deg over the several launch days centered about July 21, pseudo-conjunction. As in the 30-, 60- and 120-day curves, the peak presents some round-trip trajectory data where the return trajectory is clockwise. Immediately following these launch dates, $(V_{\infty})_T$ continues to decrease slightly without further irregularities in Fig. 14.

Fig. B-3 presents plots of $(V_{\infty})_T$ vs launch date from the Earth for the year 1971. The vertical scale of Fig. B-3 differs from that of Fig. B-2, as a result of the lower values of $(V_{\infty})_T$ occurring in 1971. In fact, since the curves are periodic, data presented in Fig. B-2 through B-11 for all the even years are plotted using scales similar to that of Fig. B-2, and data for all the odd years are plotted using scales similar to Fig. B-3. Rather than discuss Figs. B-3 through B-11 in detail, as was done with Fig. B-2, a list of peculiar variations occurring in Figs. B-2 through B-11 and the reasons for these variations are presented in Tables C-1 through C-4 of Appendix C. In general, the peaks that arise as a result of the three-dimensional analysis occur on launch dates from the Earth at the times of pseudo-conjunction, and the discontinuities or double points occur on launch dates from the Earth at the times of pseudo-opposition. Furthermore, the departure or the return trajectory is an out-of-the-ecliptic trajectory for pseudo-conjunction and a nearly rectilinear trajectory for pseudo-opposition.

On most launch dates, the round-trip trajectory consists of departure and return trajectories that are counterclockwise. However, on some specific launch dates from the Earth near the occurrence of pseudo-conjunction or pseudo-opposition, the round-trip trajectory consists of either a counterclockwise departure trajectory and a clockwise return trajectory or a clockwise departure trajectory and a counterclockwise return trajectory. The appearance of a round-trip trajectory having a one-way clockwise trajectory that yields a lower $(V_{\infty})_T$ than a round-trip trajectory consisting of two one-way counterclockwise trajectories is rather surprising. In addition, on some specific launch dates near the occurrence of pseudo-conjunction or pseudo-opposition, it is possible to have a round-trip trajectory consisting of a one-way counterclockwise trajectory and a second one-way trajectory that

can be either clockwise or counterclockwise and yet have the same flight time and $(V_{\infty})_T$.

It is interesting to note that each period for each of the four flight times contains two launch dates from the Earth on which pseudo-opposition occurs and two launch dates from the Earth on which pseudo-conjunction occurs. For Mars, opposition and conjunction occur once in approximately 2 years, so that there seems to be an inconsistency here. Actually, there is no inconsistency, since pseudo-opposition is different from opposition, and pseudo-conjunction is different from conjunction, as may be seen from the definitions in the Nomenclature. Pseudo-opposition and pseudo-conjunction each occur once for the departure trajectory and once for the return trajectory in each period of the four flight times.

The importance of a three-dimensional conic analysis is exemplified if the launch date from the Earth for the peak on the 240-day curve in Fig. B-8 is compared with the launch date from the Earth for the relative minimum $(V_{\infty})_T$ in period 4. From Tables C-4 and 2, the two dates are January 26 and January 10 in the year 1977, a difference of only 16 days. As a result, a planetary launch period centered about the launch date from the Earth for the relative minimum $(V_{\infty})_T$ in period 4 would not be desirable. However, this peak would not arise in the case of a two-dimensional conic analysis, so that the planetary launch period described above would supposedly be desirable.

During the description of Fig. B-1 near the beginning of this Section, the variation of the size of the peaks with flight time was noted. The cause of the variation of the size of the peaks cannot be determined without detailed data about the times of pseudo-conjunction. These data must be obtained from the round-trip trajectory computing program, which will be available in the near future. However, the width of the peaks is directly proportional to the celestial latitude of Mars at pseudo-conjunction. The larger the celestial latitude of Mars at pseudo-conjunction, the larger the width of the peaks. The variation of the relative minimum and maximum $(V_{\infty})_T$ in each period of a flight time curve with respect to launch date from the Earth was also noted earlier. This variation is clearly due to the changing Earth-Sun-Mars orbital geometry from period to period and is to be expected. Clarke has shown in Ref. 3 that a long-term cyclic behavior exists for one-way trajectories from Earth to Mars, which he calls the metonic cycle. This cycle is approximately 15 years in length. A similar metonic cycle exists for the case of round-trip trajectories to Mars. Since this analysis covers only a decade of the launch data from the Earth, the metonic cycle for the case of round-trip trajectories to Mars has not been determined completely.

In Section III-B it was stated that the degenerate or rectilinear one-way trajectory is impractical. This one-way trajectory is impractical because, when it occurs as a portion of a round-trip trajectory, the $(V_\infty)_r$ is much larger than the corresponding relative minimum $(V_\infty)_r$. For example, a round-trip trajectory having a nearly rectilinear one-way trajectory occurs at the discontinuities of Fig. B-1. These round-trip trajectories clearly have $(V_\infty)_r$ that are much larger than the corresponding relative minimum $(V_\infty)_r$.

This rather detailed discussion of the energy requirements for the decade 1970 to 1980 has been presented in the belief that variations of other decades are very similar for missions of the type described in this Report. In fact, by computing and adding to this analysis the appropriate data for round-trip trajectories having clockwise departure or return trajectories and the appropriate data to determine the metonic cycle completely, missions of the type described in this Report need not be studied in such detail in the future.

NOMENCLATURE

Definitions

Conjunction. A point on the orbit of a celestial body where the difference between the apparent geocentric longitudes of the celestial body and the Sun is 0 deg. If the alignment is Earth-celestial body-Sun, the celestial body is said to be in inferior conjunction with the Sun. If the alignment is Earth-Sun-celestial body, the celestial body is said to be in superior conjunction with the Sun (Ref. 4).

Double point. A point that lies on the continuous portion of a curve and that represents a double solution. The double point differs from a point of discontinuity, which also represents a double solution. See Table C-1, Table C-3, and Fig. B-1.

Earth radius. Adopted as equal to 6378.270 km (Ref. 5).

Heliocentric central angle. The angle between the heliocentric position vector of the launch planet at 0 hr of the launch date and the heliocentric position vector of the target planet at 0 hr of the arrival date.

Hohmann transfer orbit. The heliocentric ellipse that contacts tangentially both the orbit of the launch planet and of the target planet ($i = 0$ deg).

Inclination. The undirected angle between the plane of the heliocentric transfer orbit and the ecliptic plane.

Mars radius. Adopted as equal to 0.5378 Earth radii (Ref. 5).

Mass of Mars. Adopted as equal to 0.1069 Earth masses (Ref. 5).

Opposition. A point on the orbit of a celestial body where the difference between the apparent geocentric longitudes of the celestial body and the Sun is 180 deg. Note that the inner planets can never be at opposition.

Pseudo-conjunction. A point on the orbit of a target planet where the difference between the true heliocentric longitude of the target planet at arrival and the true heliocentric longitude of the launch planet at launch is 180 deg, i.e., a position of the target planet relative to a position of the launch planet at which the heliocentric central angle of the transfer orbit is 180 deg minus the sum of the celestial latitudes of the launch and target planets.

Pseudo-opposition. A point on the orbit of a target planet where the difference between the true heliocentric longitude of the target planet at arrival and the true heliocentric longitude of the launch planet at launch is 0 deg, i.e., a position of the target planet relative to a position of the launch planet at which the heliocentric central angle of the transfer orbit is 0 deg plus the absolute value of the difference of the celestial latitudes of the launch and target planets.

Stay time. The length of time a probe or spacecraft stays in orbit about the initial target planet.

Transfer orbit. The heliocentric conic that passes through the centers of the massless launch planet and target planet.

Terms used to describe a transfer orbit or trajectory

Clockwise. Motion about the Sun that is opposite to the motion of the Earth about the Sun.

Counterclockwise. Motion about the Sun that is the same as the motion of the Earth about the Sun.

Departure. Motion from the initial launch planet to the initial target planet.

Direct. Transit from the launch planet to the target planet without passing through or near a focus of the conic (primary, secondary, or both for an ellipse).

Indirect. Transit from the launch planet to the target planet passing through or near a focus of the conic (primary, secondary, or both for an ellipse).

Rectilinear. Motion along a straight line.

Return. Motion from the initial target planet to the initial launch planet.

Abbreviations

er	Earth radius
GMT	Greenwich mean time
HCA	heliocentric central angle

Subscripts

1	quantities referring to the departure trajectory
2	quantities referring to the return trajectory
\oplus	quantities referring to the Earth
σ	quantities referring to Mars
∞	quantities computed at a very large distance from the major body
c	quantities of a circular parking orbit
co	quantities of a circular parking orbit about the Earth of radius equal to the radius of the Earth
po	quantities of a parabola about the Earth with a closest approach distance equal to the radius of the Earth

Symbols

	Vectors are indicated by boldface type.
$<$	is less than
\simeq	approximately equal to

*	see Nomenclature
Δ	indicates increment
β	celestial latitude
μ	ratio of the mass of the central body to the mass of the Earth (the mass of the spacecraft is assumed negligible)
a	semimajor axis
G	gravitational constant
i	inclination relative to the ecliptic plane
k_e	geocentric gravitational constant ($k_e^2 = G M_\oplus$)
M	mass
r	radius distance of the parking orbit
R	heliocentric radius distance
V	speed
V_\oplus	heliocentric speed of the Earth
$(V_1)_{\oplus\oplus}$	heliocentric take-off speed from the Earth
$(V_2)_{\sigma\oplus}$	heliocentric take-off speed from Mars
$(V_1)_\oplus$	take-off speed from the Earth
$(V_2)_\oplus$	approach speed to the Earth
$(V_\infty)_{\oplus 1}$	hyperbolic excess speed relative to the Earth, going to Mars
$(V_\infty)_{\oplus 2}$	hyperbolic excess speed relative to the Earth, returning to Earth
$(V_\infty)_{\sigma 1}$	hyperbolic excess speed relative to Mars, going to Mars
$(V_\infty)_{\sigma 2}$	hyperbolic excess speed relative to Mars, returning to Earth
$(V_1)_\sigma$	approach speed to Mars
$(V_2)_\sigma$	take-off speed from Mars
$(V_c)_\oplus$	speed in the circular orbit about the Earth
$(V_c)_\sigma$	speed in the circular orbit about Mars
$(V_p)_\oplus$	speed in a parabolic orbit about Earth
$(V_p)_\sigma$	speed in a parabolic orbit about Mars
$(V_\infty)_T$	total hyperbolic excess speed
$(\Delta V)_T$	total speed increment required
T_F	time of flight (one way)

Units of measurement

Angles	degrees	Mass	Earth masses
		Speed	kilometers per second
Distance	kilometers or Earth radii (er)	Time	seconds or days

REFERENCES

1. Clarke, V. C., Jr., Roth, R. Y., Bollman, W. E., Hamilton, T. H., and Pfeiffer, C. G., *Earth-Mars Trajectories, 1964*, Technical Memorandum No. 33-100, Vol. 1, Part A, Jet Propulsion Laboratory, Pasadena, California, March 1, 1964.
2. Bollman, W. E., *The Engineering Design of Interplanetary Ballistic Trajectories*, AIAA Report No. 63-414, August 19-21, 1963.
3. Clarke, V. C., Jr., *A Summary of the Characteristics of Ballistic Interplanetary Trajectories, 1962-1977*, Technical Report No. 32-209, Jet Propulsion Laboratory, Pasadena, California, January 15, 1962.
4. *Explanatory Supplement to the Ephemeris*, Her Majesty's Stationery Office, London, 1961.
5. Herrick, Samuel, *Astroynamics*, Van Nostrand, New York, In press.

APPENDIX A

Calculation of Exact and Approximate Expressions for $(\Delta V)_T$ I. EXACT EXPRESSION FOR $(\Delta V)_T$

From the design constraints listed in Table 1 and Ref. 5,

$$\left. \begin{array}{lll} \mu_{\oplus} = 1,^* & r_{\oplus} = 1.1 \text{ er},^* & V_{co} = 7.905 \text{ km/sec} \\ \mu_{\odot} = 0.1069 & r_{\odot} = 0.5916 \text{ er}, & V_{po} = 11.180 \text{ km/sec} \\ & 1 \text{ Mars radius} = 0.5378 \text{ er} \end{array} \right\} \quad (\text{A-1})$$

and from the vis viva integral with μ in Earth masses and with r and a in Earth radii,

$$V^2 = k_e^2 \mu \left(\frac{2}{r} - \frac{1}{a} \right) \quad (\text{A-2})$$

$$V_{co} = k_e, V_{po} = k_e (2)^{1/2}. \quad (\text{A-3})$$

Therefore,

$$\left. \begin{array}{ll} (V_p)_{\oplus}^2 = V_{po}^2 \left(\frac{\mu_{\oplus}}{r_{\oplus}} \right), & (V_c)_{\oplus}^2 = V_{co}^2 \left(\frac{\mu_{\oplus}}{r_{\oplus}} \right) \\ (V_p)_{\odot}^2 = V_{po}^2 \left(\frac{\mu_{\odot}}{r_{\odot}} \right), & (V_c)_{\odot}^2 = V_{co}^2 \left(\frac{\mu_{\odot}}{r_{\odot}} \right) \end{array} \right\} \quad (\text{A-4})$$

For the Earth-to-Mars requirements, departure,

$$\left. \begin{array}{ll} (V_1)_{\oplus}^2 = (V_{\infty})_{\oplus 1}^2 + (V_p)_{\oplus}^2, & (V_1)_{\odot}^2 = (V_{\infty})_{\odot 1}^2 + (V_p)_{\odot}^2 \\ (\Delta V_1)_{\oplus} = (V_1)_{\oplus} - (V_c)_{\oplus}, & (\Delta V_1)_{\odot} = (V_1)_{\odot} - (V_c)_{\odot} \end{array} \right\} \quad (\text{A-5})$$

For the Mars-to-Earth requirements, return,

$$\left. \begin{array}{ll} (V_2)_{\odot}^2 = (V_{\infty})_{\odot 2}^2 + (V_p)_{\odot}^2, & (V_2)_{\oplus}^2 = (V_{\infty})_{\oplus 2}^2 + (V_p)_{\oplus}^2 \\ (\Delta V_2)_{\odot} = (V_2)_{\odot} - (V_c)_{\odot}, & (\Delta V_2)_{\oplus} = (V_2)_{\oplus} - (V_c)_{\oplus} \end{array} \right\} \quad (\text{A-6})$$

Finally, from Fig. 1 and Eqs. (A-1) through (A-6),

$$(\Delta V)_T = (\Delta V_1)_{\oplus} + (\Delta V_1)_{\odot} + (\Delta V_2)_{\odot} + (\Delta V_2)_{\oplus}$$

or

$$\begin{aligned} (\Delta V)_T = & [(V_{\infty})_{\oplus 1}^2 + (V_p)_{\oplus}^2]^{1/2} + [(V_{\infty})_{\odot 1}^2 + (V_p)_{\odot}^2]^{1/2} \\ & + [(V_{\infty})_{\oplus 2}^2 + (V_p)_{\oplus}^2]^{1/2} + [(V_{\infty})_{\odot 2}^2 + (V_p)_{\odot}^2]^{1/2} - 2 [(V_c)_{\oplus} + (V_c)_{\odot}]. \end{aligned} \quad (\text{A-7})$$

Hence, for the design constraints chosen in this analysis,

$$\begin{aligned}
 (\Delta V)_T = & [(V_\infty)_{\oplus 1}^2 + 113.629]^{1/2} + [(V_\infty)_{\sigma 1}^2 + 22.586]^{1/2} \\
 & + [(V_\infty)_{\sigma 2}^2 + 22.586]^{1/2} + [(V_\infty)_{\oplus 2}^2 + 113.629]^{1/2} - 21.794.
 \end{aligned} \tag{A-8}$$

II. APPROXIMATE EXPRESSIONS FOR $(\Delta V)_T$

From Section III-D,

$$(V_\infty)_T = (V_\infty)_{\oplus 1} + (V_\infty)_{\sigma 1} + (V_\infty)_{\sigma 2} + (V_\infty)_{\oplus 2}. \tag{A-9}$$

Consider the case of a fast flight time so that

$$(V_\infty)_{\oplus 1} > (V_p)_{\oplus}, (V_\infty)_{\sigma 1} > (V_p)_{\sigma}, (V_\infty)_{\sigma 2} > (V_p)_{\sigma}, (V_\infty)_{\oplus 2} > (V_p)_{\oplus}. \tag{A-10}$$

From Eq. (A-7),

$$\begin{aligned}
 (\Delta V)_T = & (V_\infty)_{\oplus 1} \left\{ 1 + \left[\frac{(V_p)_{\oplus}}{(V_\infty)_{\oplus 1}} \right]^2 \right\}^{1/2} + (V_\infty)_{\sigma 1} \left\{ 1 + \left[\frac{(V_p)_{\sigma}}{(V_\infty)_{\sigma 1}} \right]^2 \right\}^{1/2} \\
 & + (V_\infty)_{\sigma 2} \left\{ 1 + \left[\frac{(V_p)_{\sigma}}{(V_\infty)_{\sigma 2}} \right]^2 \right\}^{1/2} + (V_\infty)_{\oplus 2} \left\{ 1 + \left[\frac{(V_p)_{\oplus}}{(V_\infty)_{\oplus 2}} \right]^2 \right\}^{1/2} \\
 & - 2 [(V_c)_{\oplus} + (V_c)_{\sigma}].
 \end{aligned} \tag{A-11}$$

Using the binomial expansion for the square roots that is permitted because of the inequalities (A-10), Eq. (A-11) becomes

$$\begin{aligned}
 (\Delta V)_T = & (V_\infty)_{\oplus 1} \left\{ 1 + \frac{1}{2} \left[\frac{(V_p)_{\oplus}}{(V_\infty)_{\oplus 1}} \right]^2 + \dots \right\} + (V_\infty)_{\sigma 1} \left\{ 1 + \frac{1}{2} \left[\frac{(V_p)_{\sigma}}{(V_\infty)_{\sigma 1}} \right]^2 + \dots \right\} \\
 & + (V_\infty)_{\sigma 2} \left\{ 1 + \frac{1}{2} \left[\frac{(V_p)_{\sigma}}{(V_\infty)_{\sigma 2}} \right]^2 + \dots \right\} + (V_\infty)_{\oplus 2} \left\{ 1 + \frac{1}{2} \left[\frac{(V_p)_{\oplus}}{(V_\infty)_{\oplus 2}} \right]^2 + \dots \right\} \\
 & - 2 [(V_c)_{\oplus} + (V_c)_{\sigma}]
 \end{aligned}$$

or

$$\begin{aligned}
 (\Delta V)_T = & [(V_\infty)_{\oplus 1} + (V_\infty)_{\sigma 1} + (V_\infty)_{\sigma 2} + (V_\infty)_{\oplus 2}] \\
 & + \frac{1}{2} \left[\frac{(V_p)_{\oplus}^2}{(V_\infty)_{\oplus 1}} + \frac{(V_p)_{\sigma}^2}{(V_\infty)_{\sigma 1}} + \frac{(V_p)_{\sigma}^2}{(V_\infty)_{\sigma 2}} + \frac{(V_p)_{\oplus}^2}{(V_\infty)_{\oplus 2}} \right] \\
 & + \dots - 2 [(V_c)_{\oplus} + (V_c)_{\sigma}].
 \end{aligned} \tag{A-12}$$

From Eqs. (A-9) and (A-12),

$$(\Delta V)_T = (V_\infty)_T - 2[(V_c)_\oplus + (V_c)_\odot] \\ + \frac{1}{2} \left[\frac{(V_p)_\oplus^2}{(V_\infty)_{\oplus 1}} + \frac{(V_p)_\odot^2}{(V_\infty)_{\odot 1}} + \frac{(V_p)_\odot^2}{(V_\infty)_{\odot 2}} + \frac{(V_p)_\oplus^2}{(V_\infty)_{\oplus 2}} \right] + \dots$$

and for a sufficiently fast flight time,

$$(\Delta V)_T = (V_\infty)_T - 2 [(V_c)_\oplus + (V_c)_\odot] . \quad (A-13)$$

Consider the case where $(V_\infty)_T = 0$. From Eq. (A-9),

$$(V_\infty)_T = (V_\infty)_{\oplus 1} + (V_\infty)_{\odot 1} + (V_\infty)_{\odot 2} + (V_\infty)_{\oplus 2} = 0 . \quad (A-14)$$

Equation (A-14) implies, since V_∞ is a speed and therefore greater than or equal to zero, that $(V_\infty)_{\oplus 1} = (V_\infty)_{\odot 1} = (V_\infty)_{\odot 2} = (V_\infty)_{\oplus 2} = 0$. For this case, Eq. (A-7)

becomes

$$(\Delta V)_T = 2 [(V_p)_\oplus + (V_p)_\odot] - 2 [(V_c)_\oplus + (V_c)_\odot] . \quad (A-15)$$

From Eqs. (A-4) and (A-15),

$$(\Delta V)_T = 2 \left[\frac{V_{p0}}{V_{c0}} (V_c)_\oplus + \frac{V_{p0}}{V_{c0}} (V_c)_\odot \right] - 2 [(V_c)_\oplus + (V_c)_\odot]$$

and using Eqs. (A-3),

$$(\Delta V)_T = 2 [(2)^{1/2} (V_c)_\oplus + (2)^{1/2} (V_c)_\odot] - 2 [(V_c)_\oplus + (V_c)_\odot]$$

or

$$(\Delta V)_T = 0.828 [(V_c)_\oplus + (V_c)_\odot] . \quad (A-16)$$

Hence, for the design constraints chosen in this analysis,

$$(\Delta V)_T = (0.828) [7.537 + 3.360] = 9.027 . \quad (A-17)$$

APPENDIX B

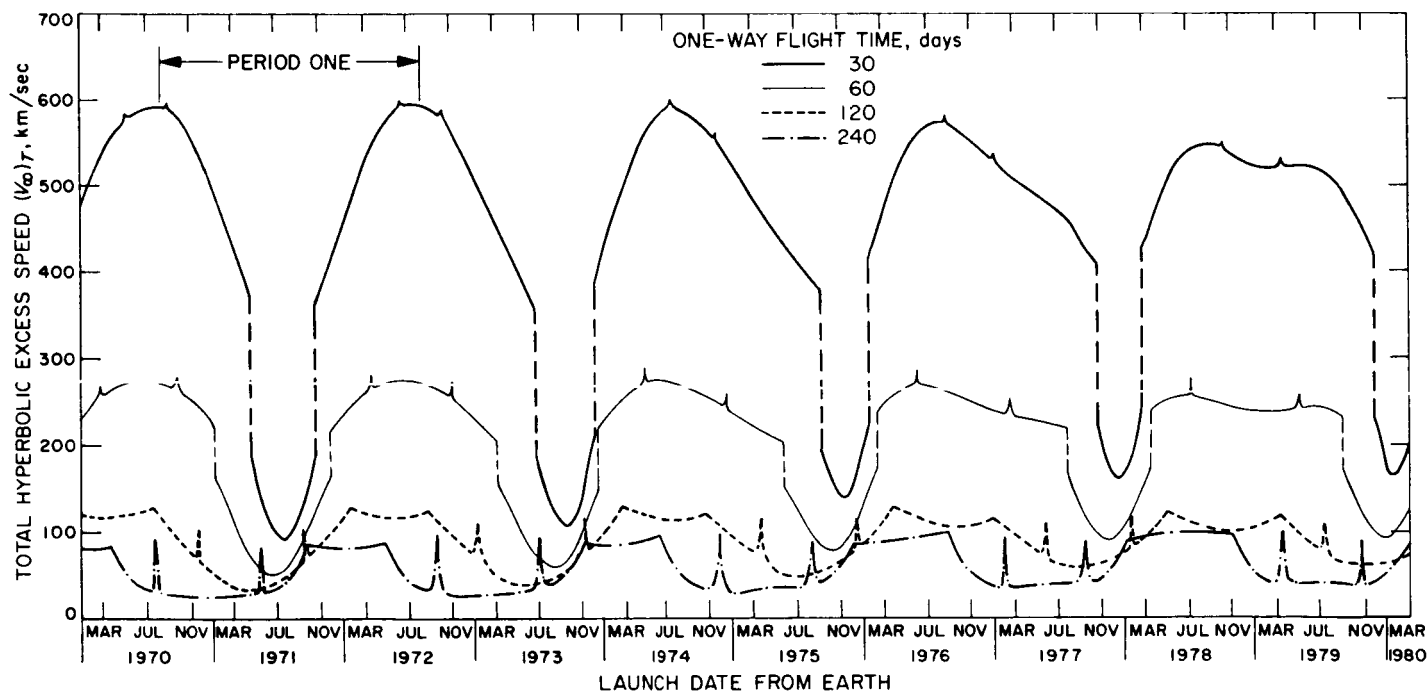
Plots of $(V_{\infty})_T$ and $(\Delta V)_T$ vs Launch Date From the Earth in the Decade 1970 to 1980

Fig. B-1. Earth-Mars-Earth trajectories, 1970 to 1980, sum of geocentric and aerocentric hyperbolic excess speeds vs launch date

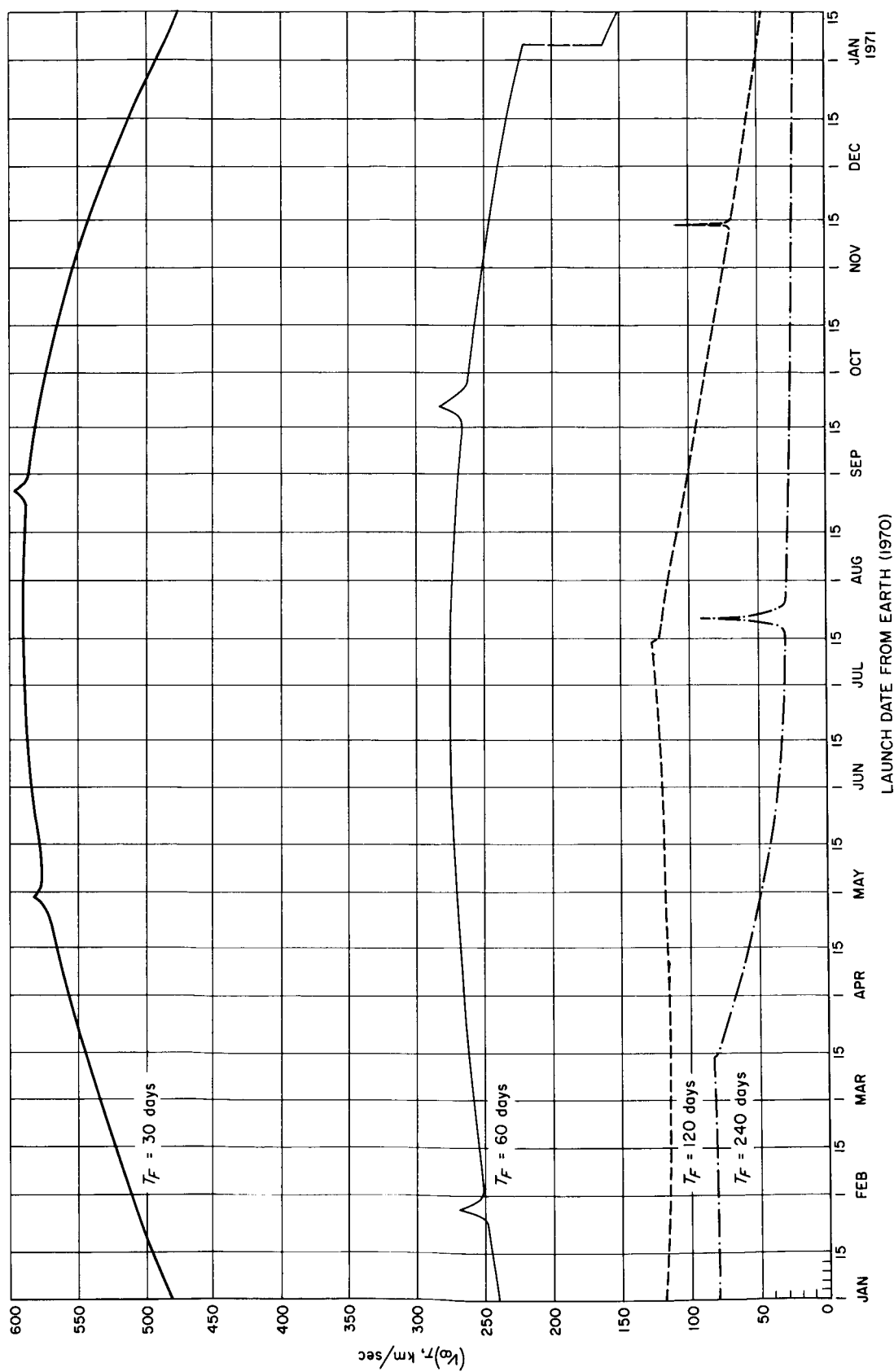


Fig. B-2. Earth-Mars-Earth trajectories, 1970, sum of geocentric and areocentric hyperbolic excess speeds vs launch date

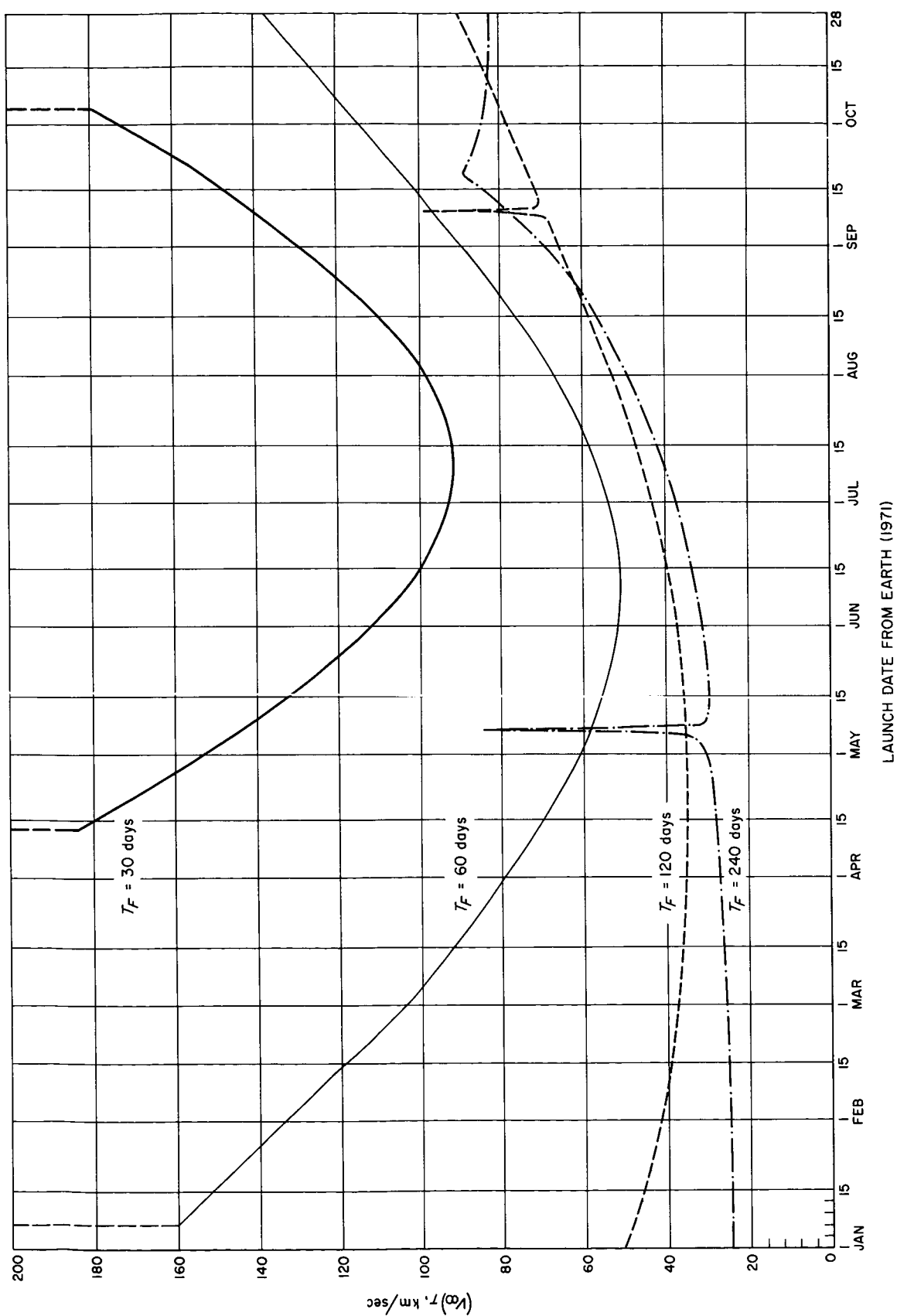


Fig. B-3. Earth-Mars-Earth trajectories, 1971, sum of geocentric and areocentric hyperbolic excess speeds vs launch date

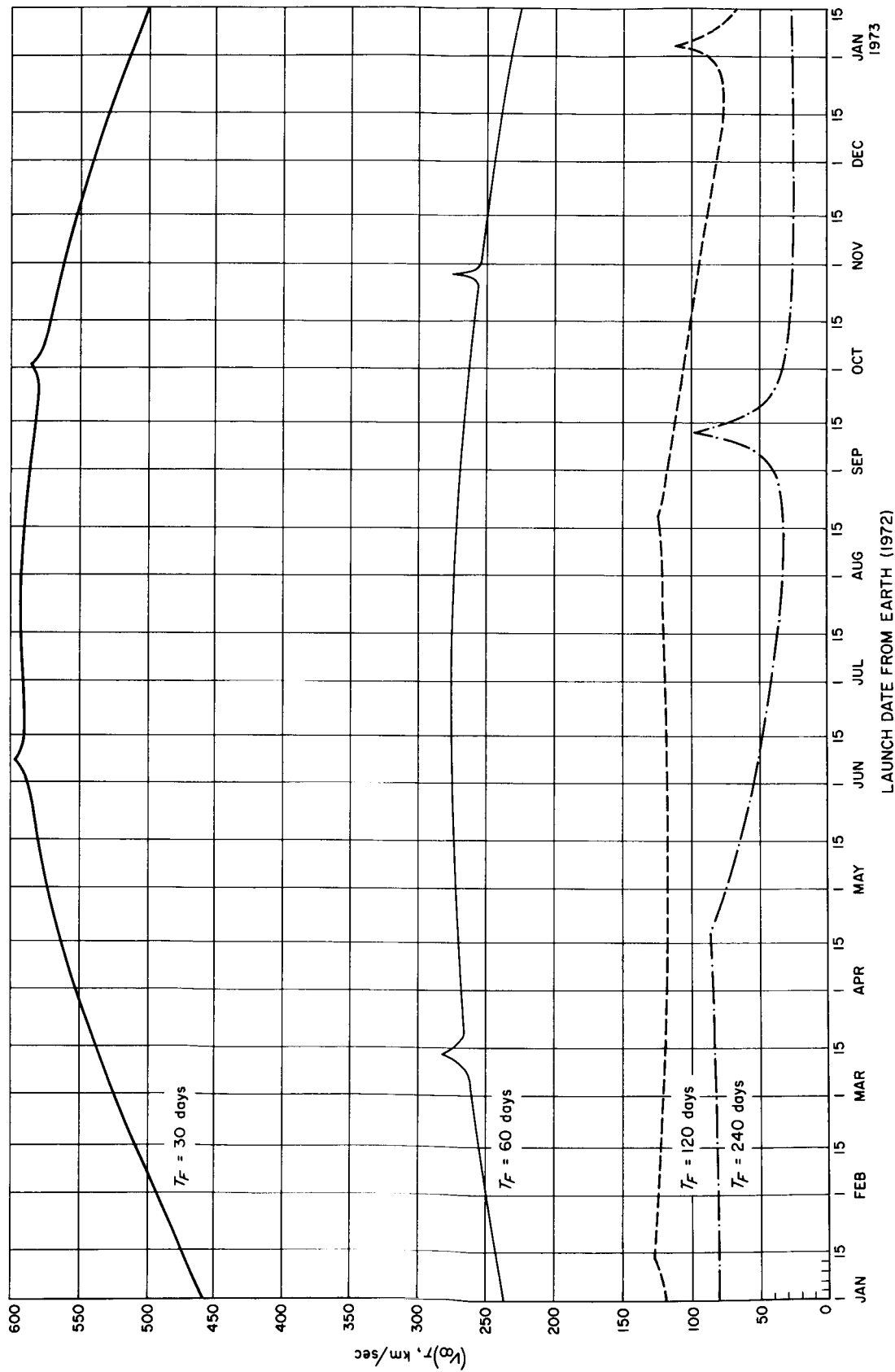


Fig. B-4. Earth-Mars-Earth trajectories, 1972, sum of geocentric and areocentric hyperbolic excess speeds vs launch date

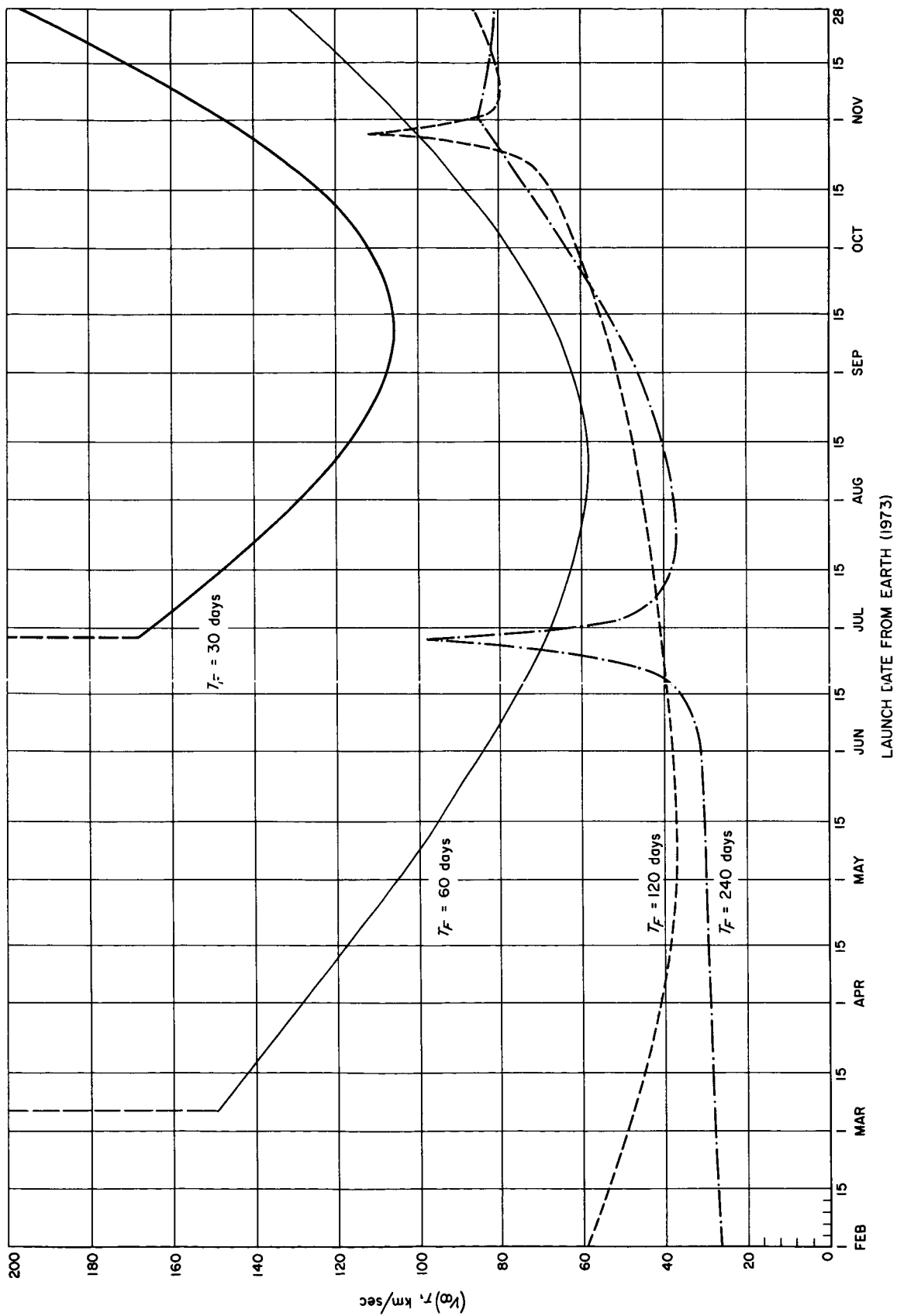


Fig. B-5. Earth-Mars-Earth trajectories, 1973, sum of geocentric and areocentric hyperbolic excess speeds vs launch date

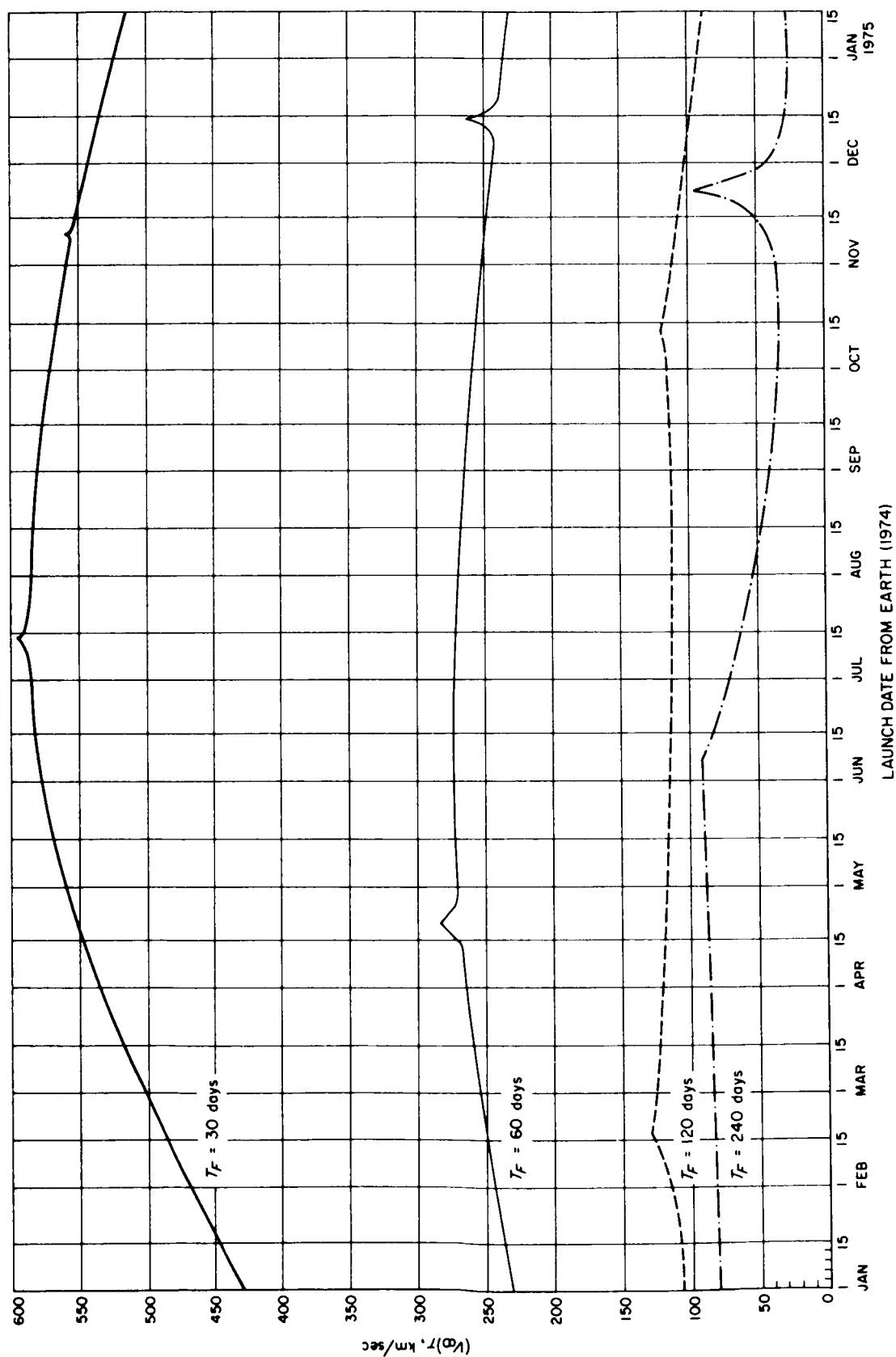


Fig. B-6. Earth-Mars-Earth trajectories, 1974, sum of geocentric and areocentric hyperbolic excess speeds vs launch date

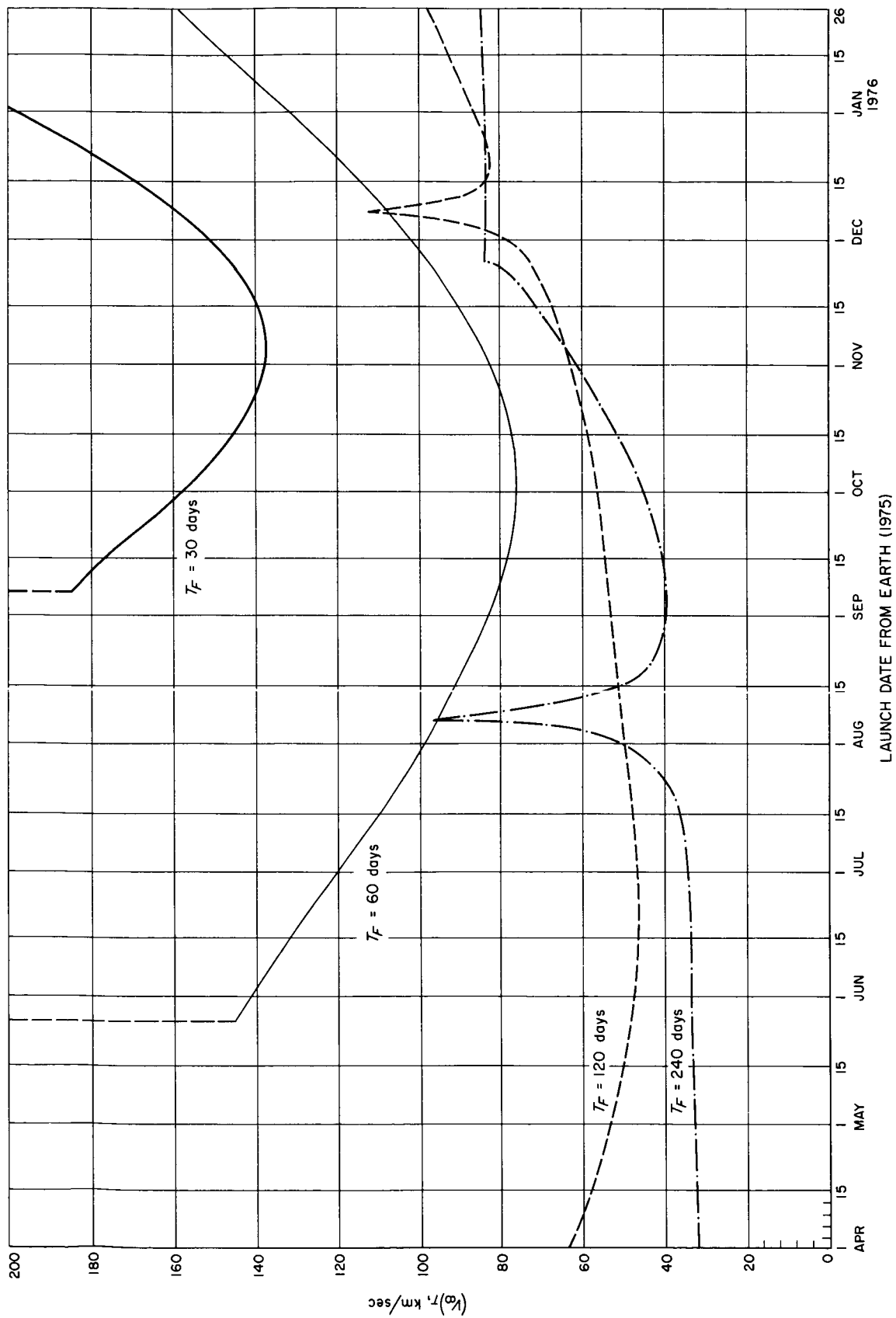


Fig. B-7. Earth-Mars trajectories, 1975, sum of geocentric and areocentric hyperbolic excess speeds vs launch date

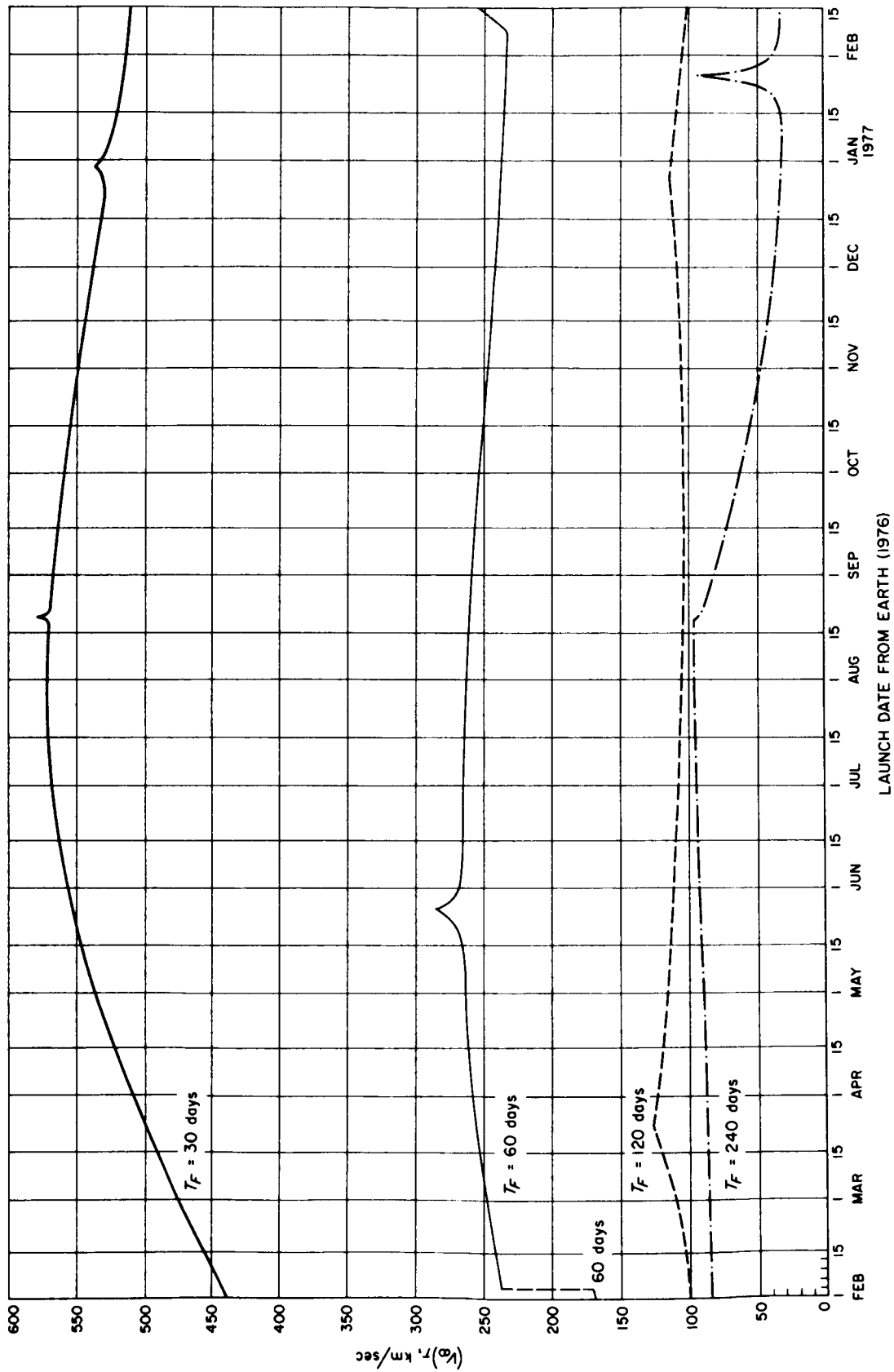


Fig. B-8. Earth-Mars-Earth trajectories, 1976, sum of geocentric and areocentric hyperbolic excess speeds vs launch date

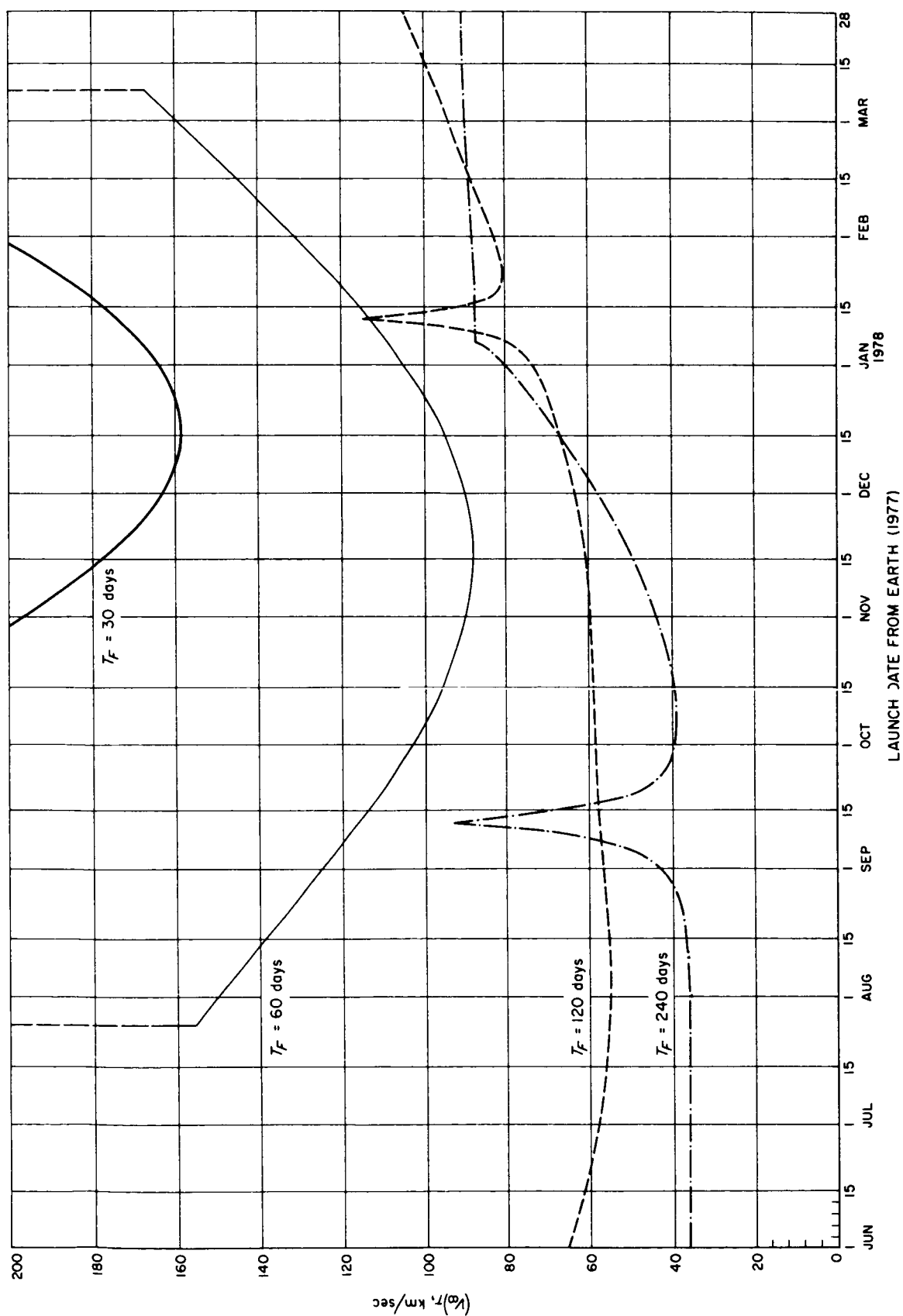


Fig. B-9. Earth-Mars-Earth trajectories, 1977, sum of geocentric and areocentric hyperbolic excess speeds vs launch date

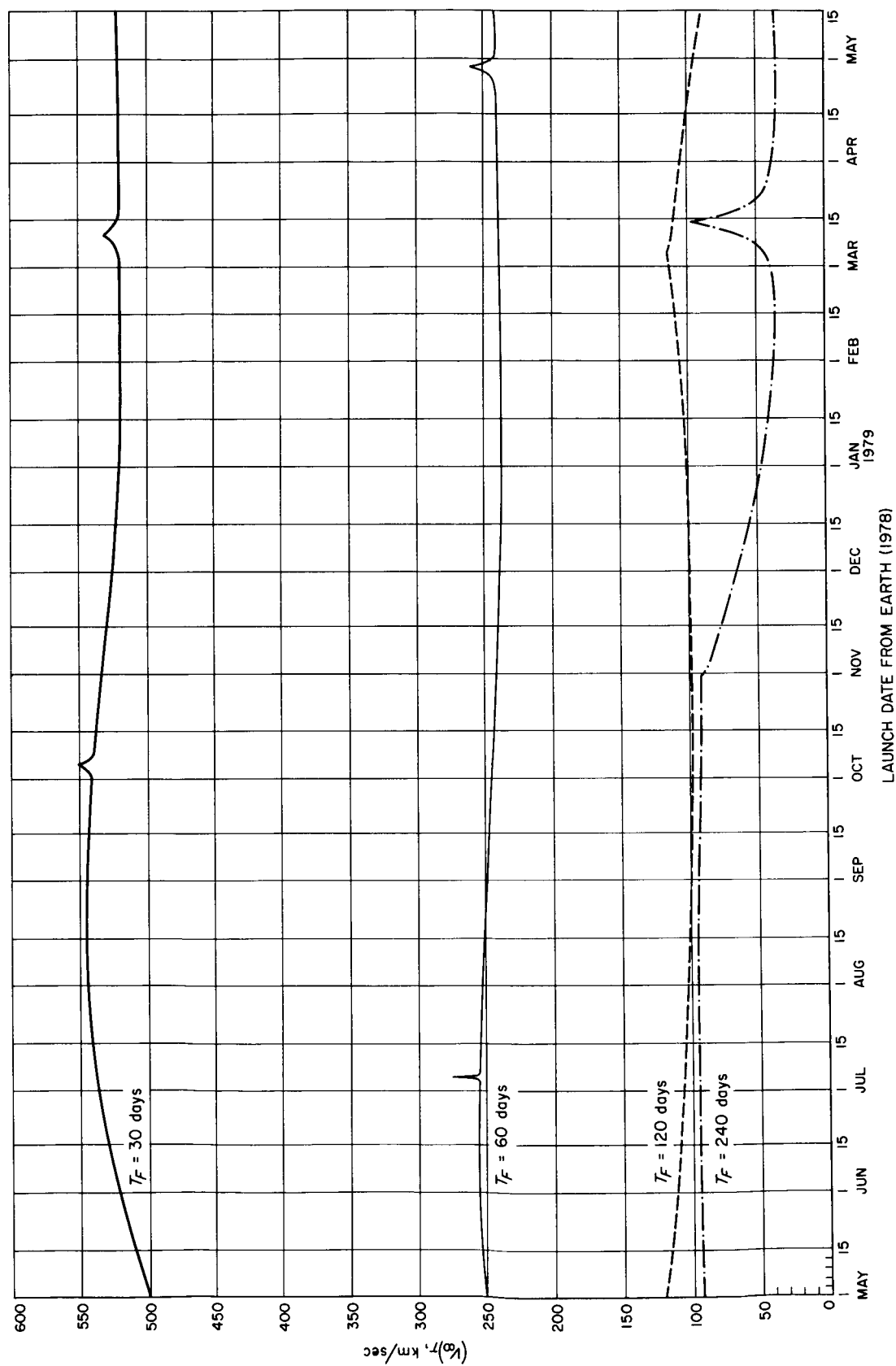


Fig. B-10. Earth-Mars-Earth trajectories, 1978, sum of geocentric and areocentric hyperbolic excess speeds vs launch date

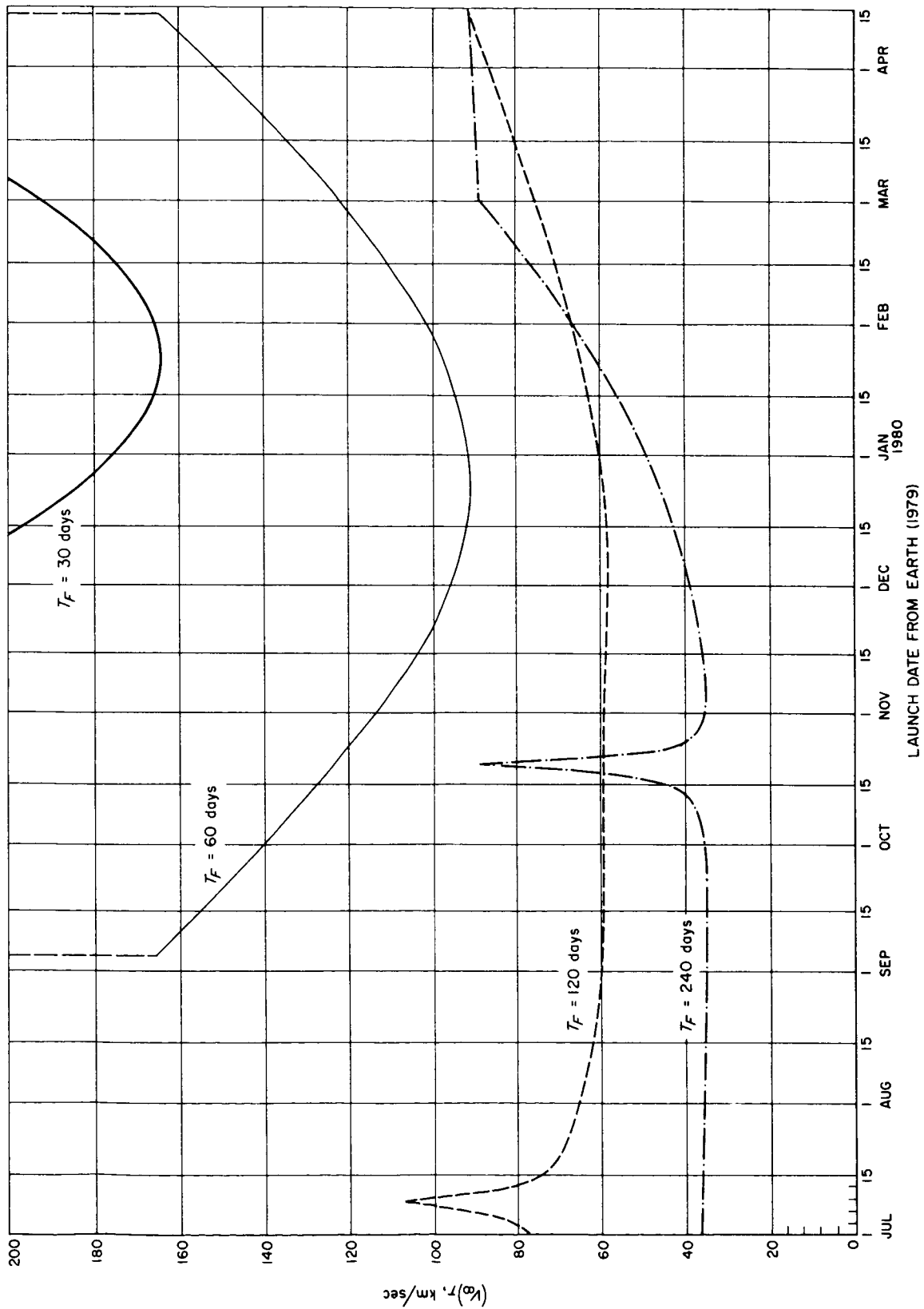


Fig. B-11. Earth-Mars-Earth trajectories, 1979, sum of geocentric and areocentric hyperbolic excess speeds vs launch date

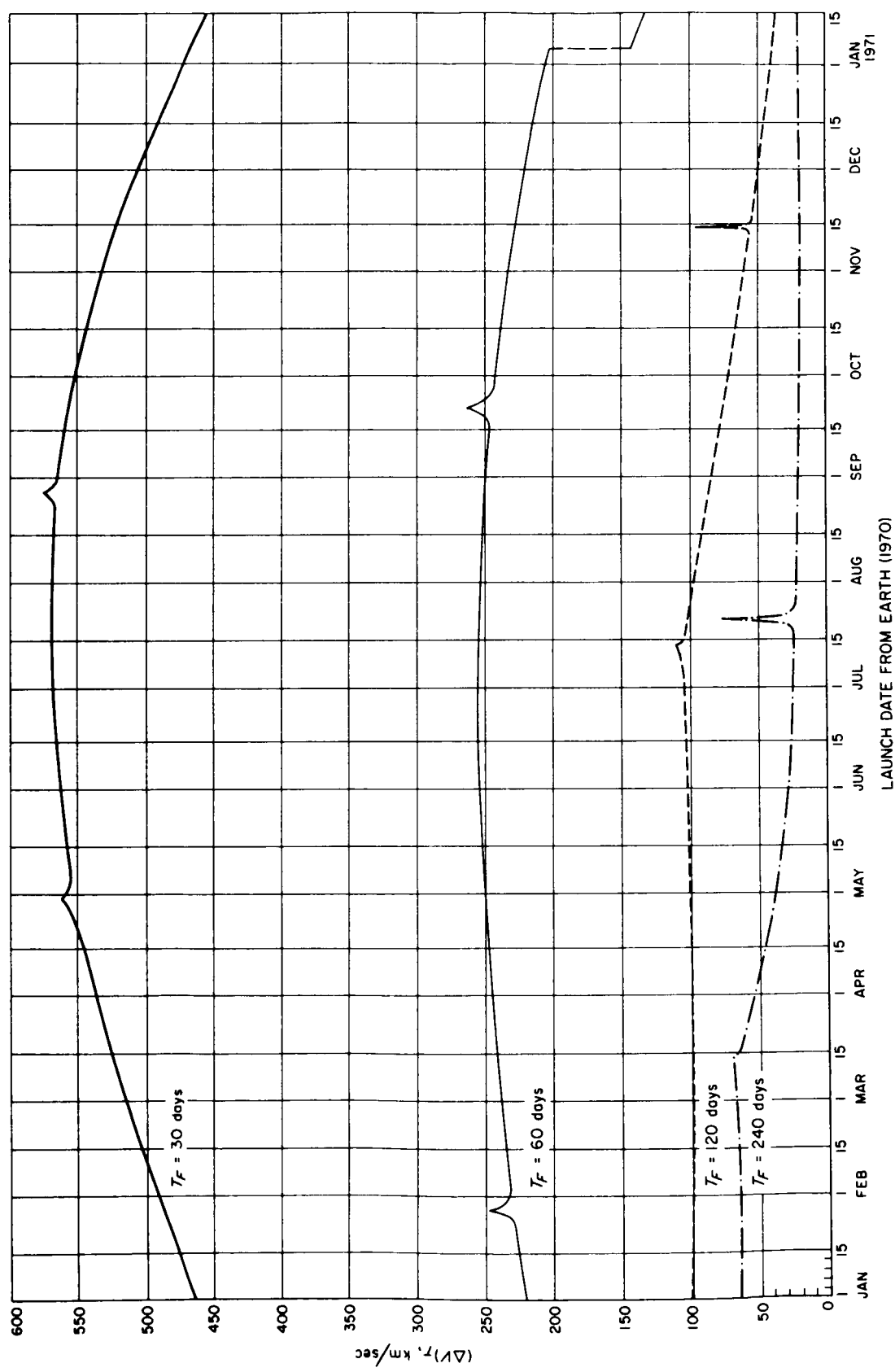


Fig. B-12. Earth-Mars-Earth trajectories, 1970, total speed increment from Earth orbit to Mars orbit to Earth orbit vs launch date

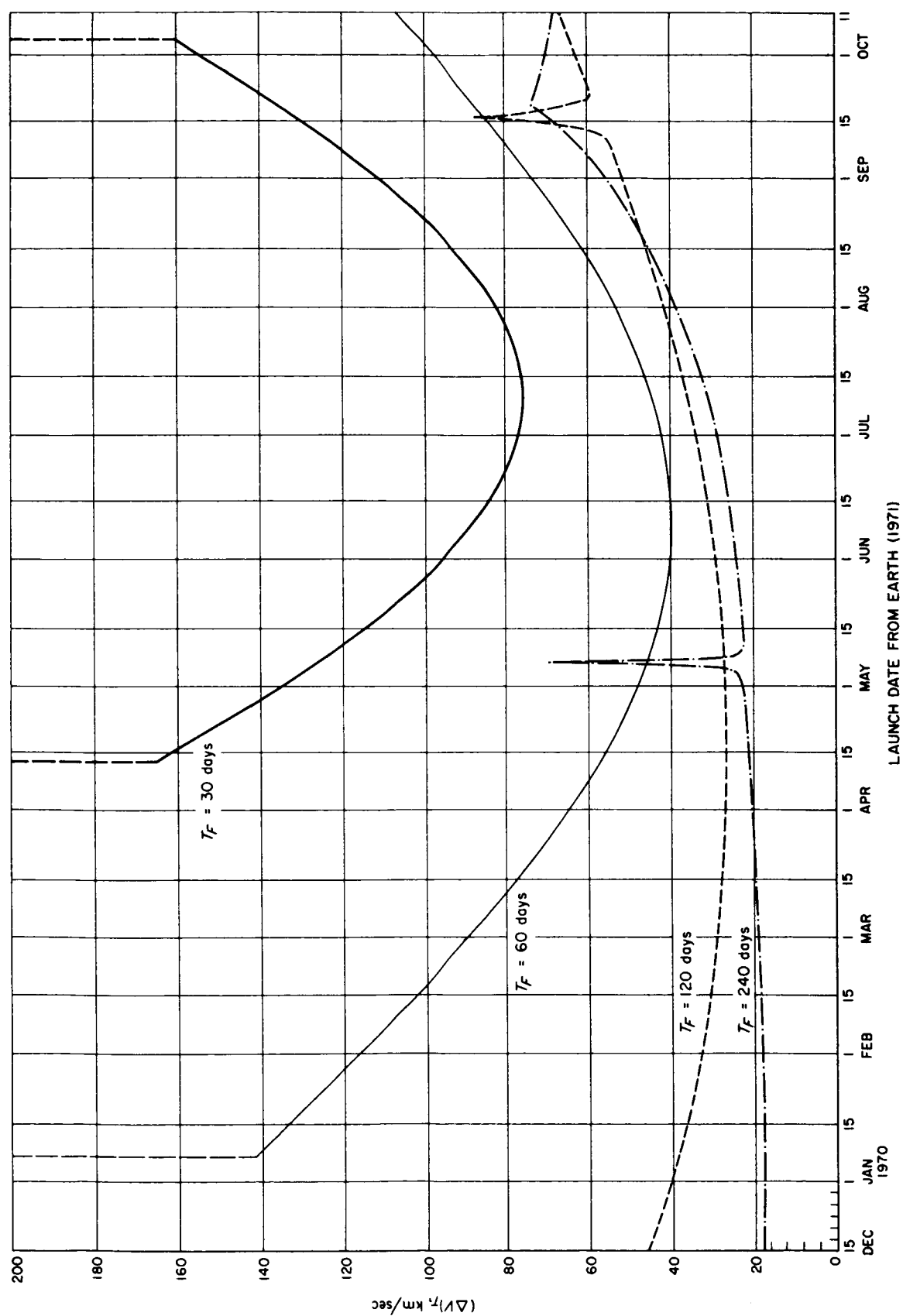


Fig. B-13. Earth-Mars-Earth trajectories, 1971, total speed increment from Earth orbit to Mars orbit to Earth orbit vs launch date

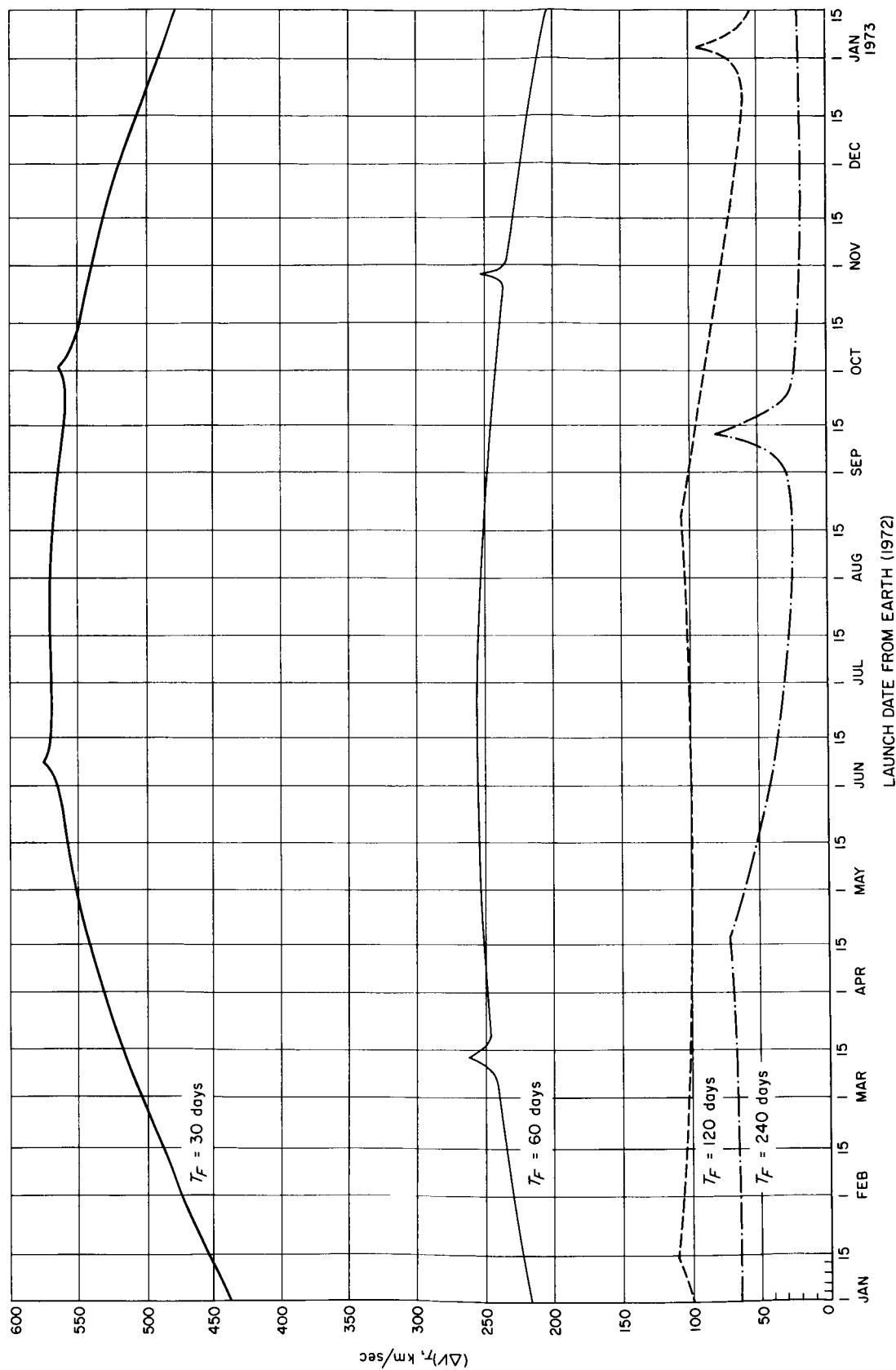


Fig. B-14. Earth-Mars-Earth trajectories, 1972, total speed increment from Earth orbit to Mars orbit to Earth orbit vs launch date

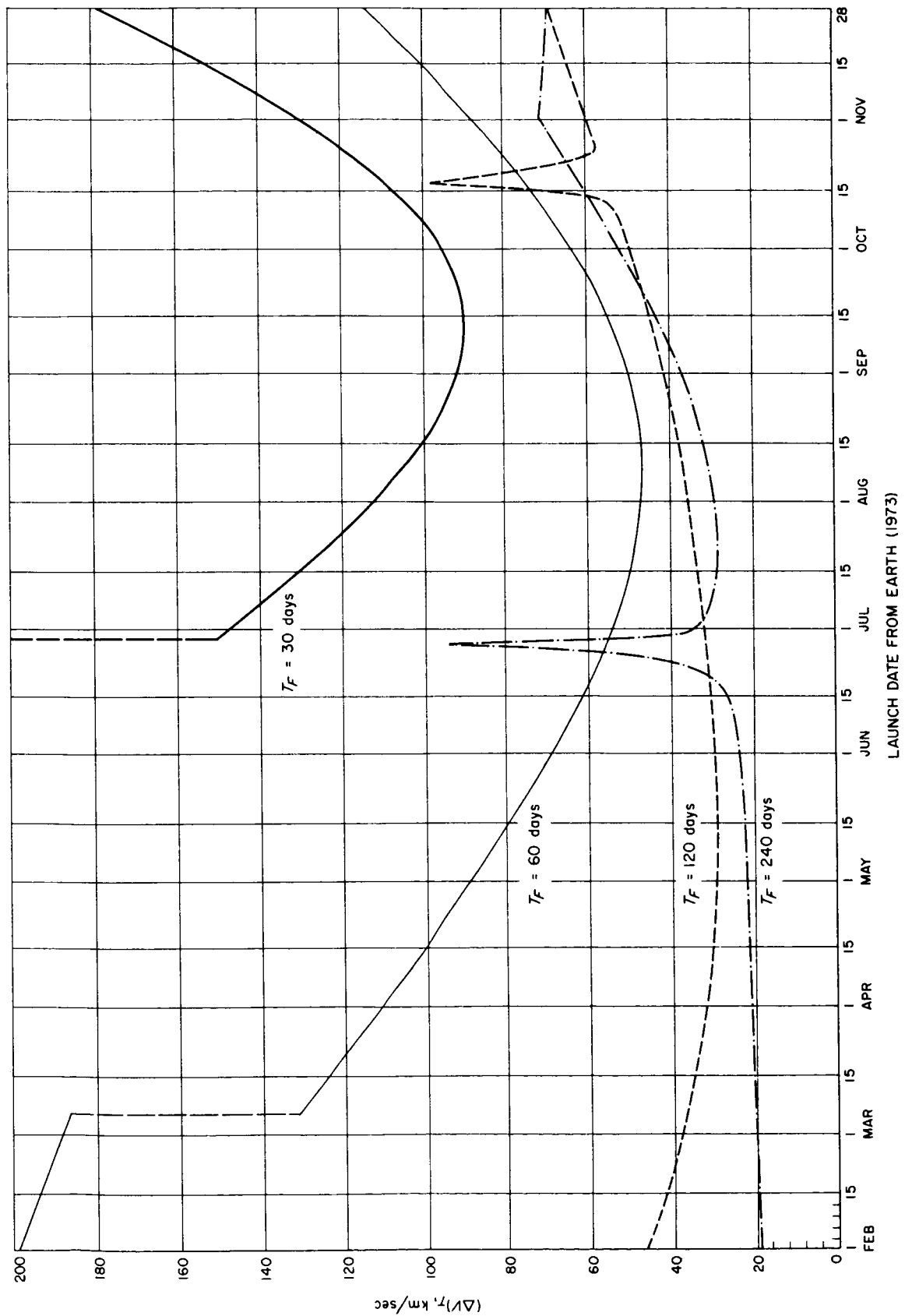


Fig. B-15. Earth-Mars-Earth trajectories, 1973, total speed increment from Earth orbit to Mars orbit to Earth orbit vs launch date

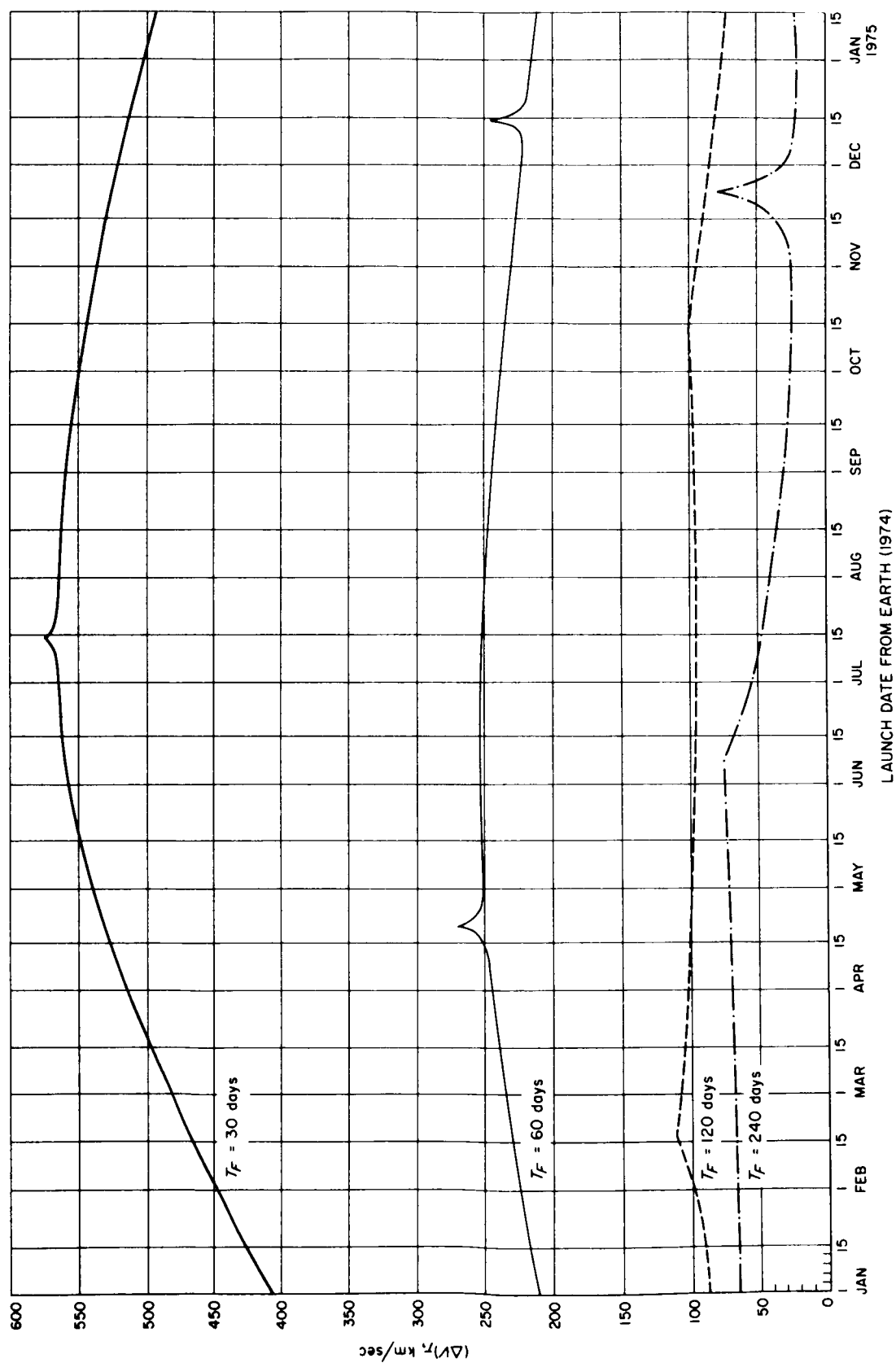


Fig. B-16. Earth-Mars-Earth trajectories, 1974, total speed increment from Earth orbit to Mars orbit to Earth orbit vs launch date

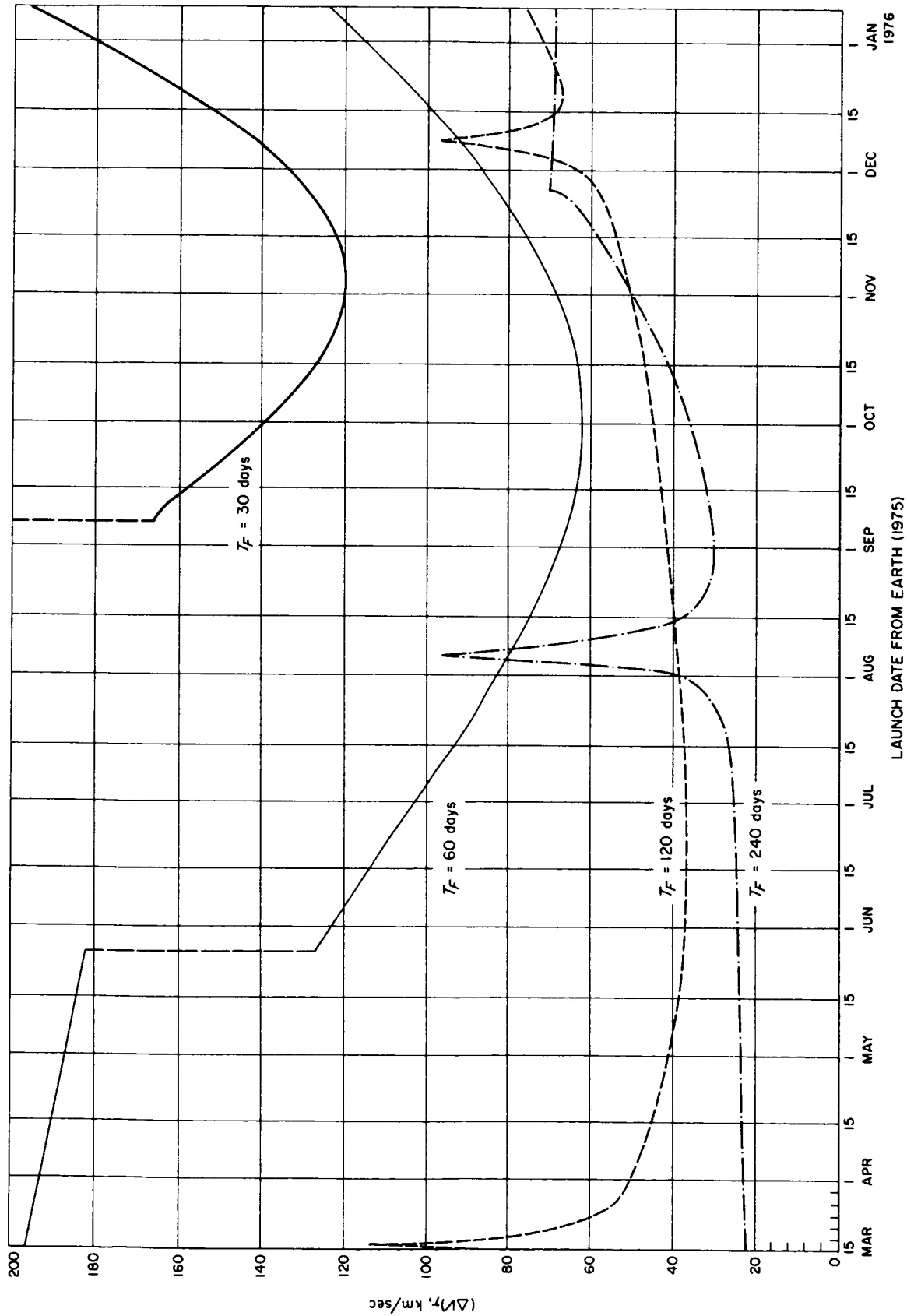


Fig. B-17. Earth-Mars-Earth trajectories, 1975, total speed increment from Earth orbit to Mars orbit vs launch date

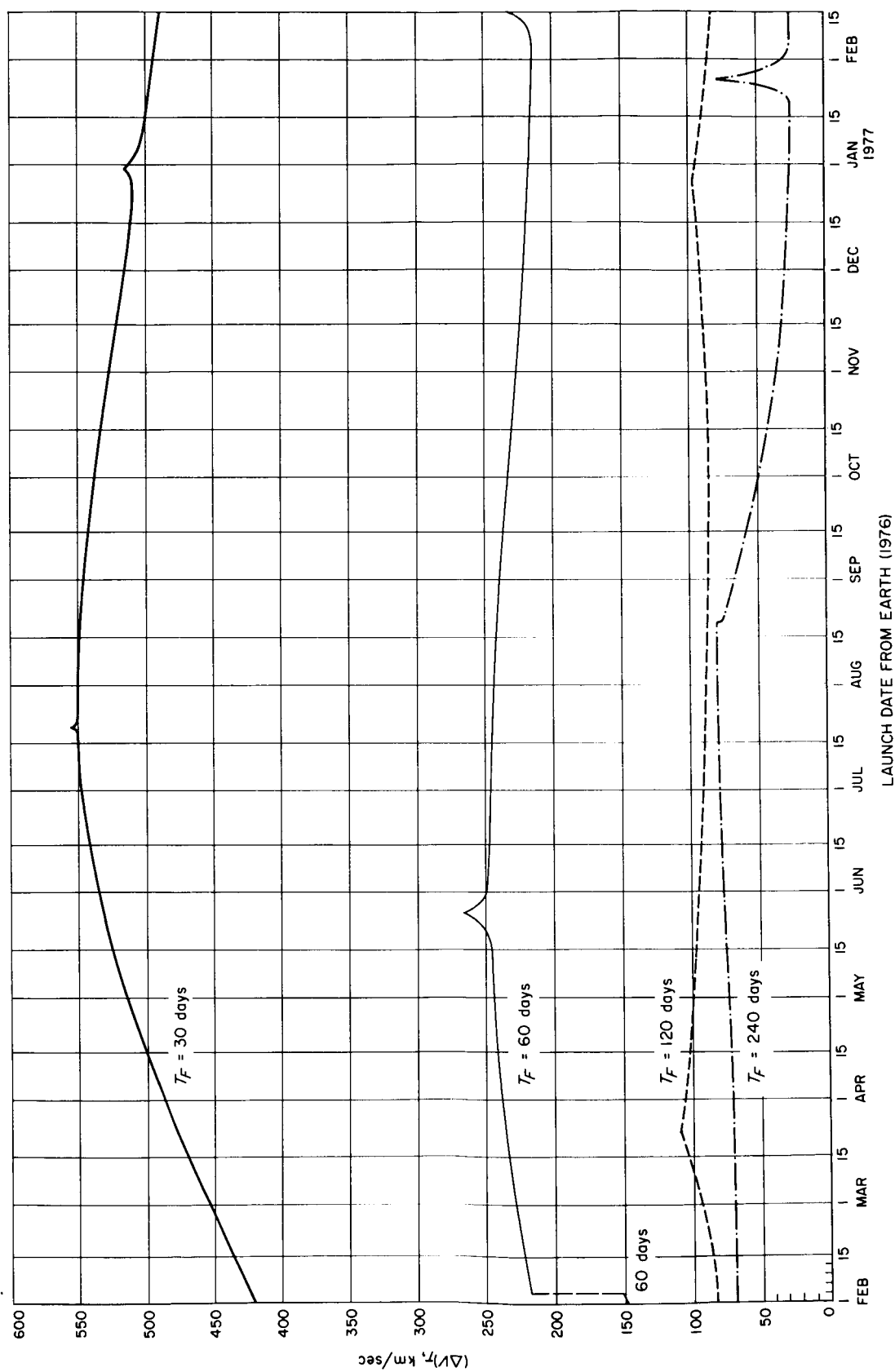


Fig. B-18. Earth-Mars-Earth trajectories, 1976, total speed increment from Earth orbit to Mars orbit vs launch date

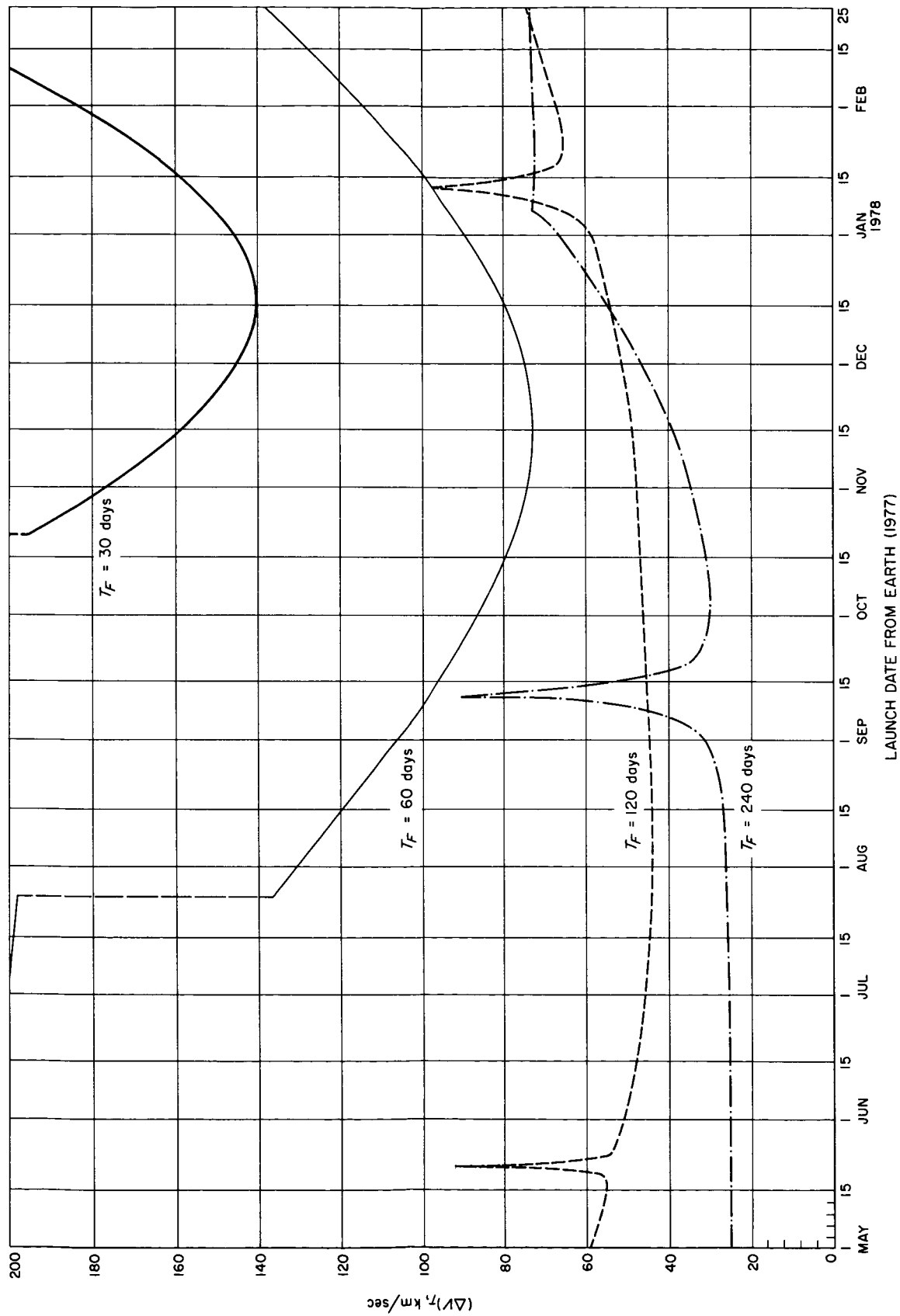


Fig. B-19. Earth-Mars-Earth trajectories, 1977, total speed increment from Earth orbit to Mars orbit vs launch date

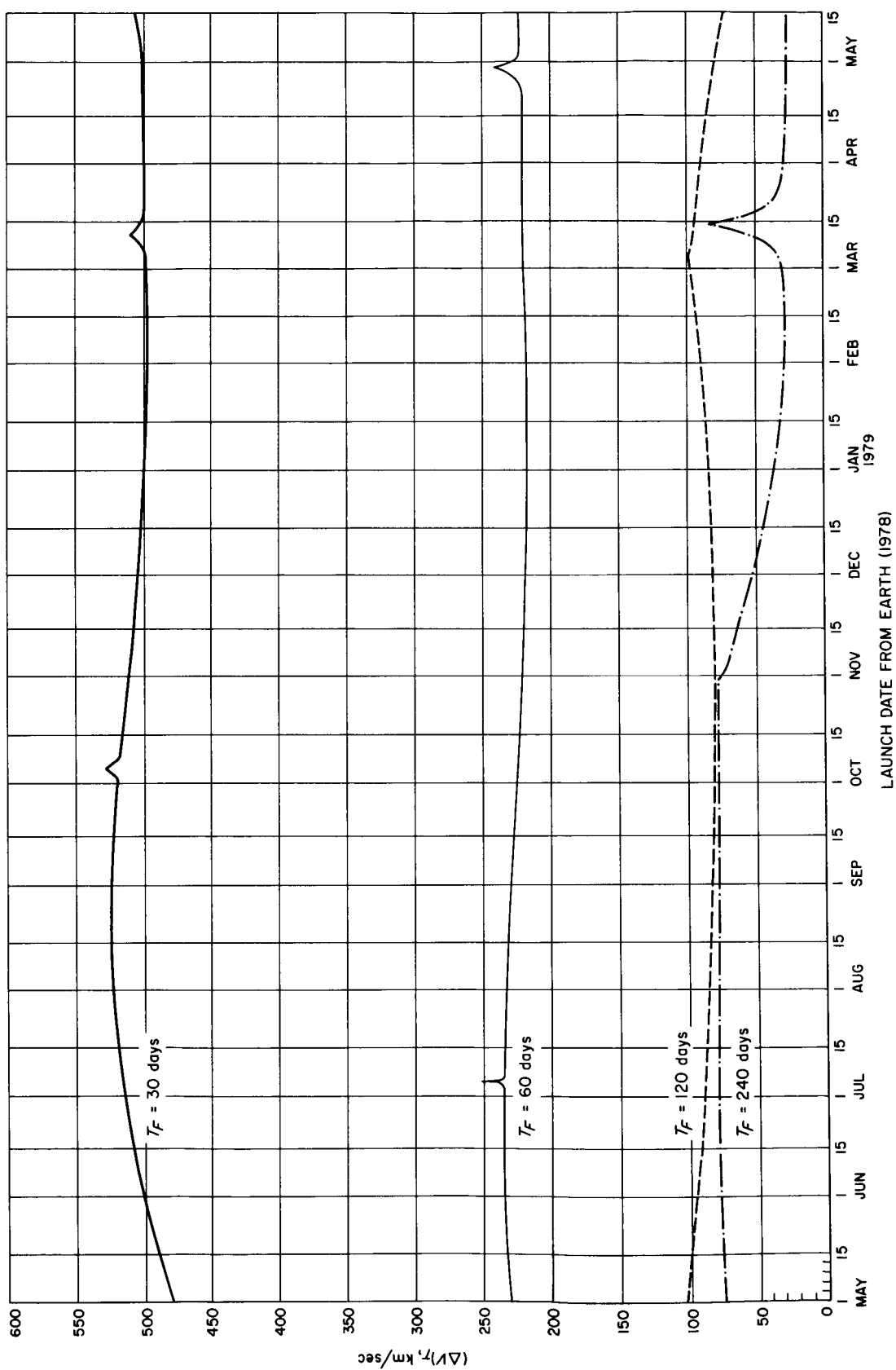


Fig. B-20. Earth-Mars-Earth trajectories, 1978, total speed increment from Earth orbit to Mars orbit to Earth orbit vs launch date

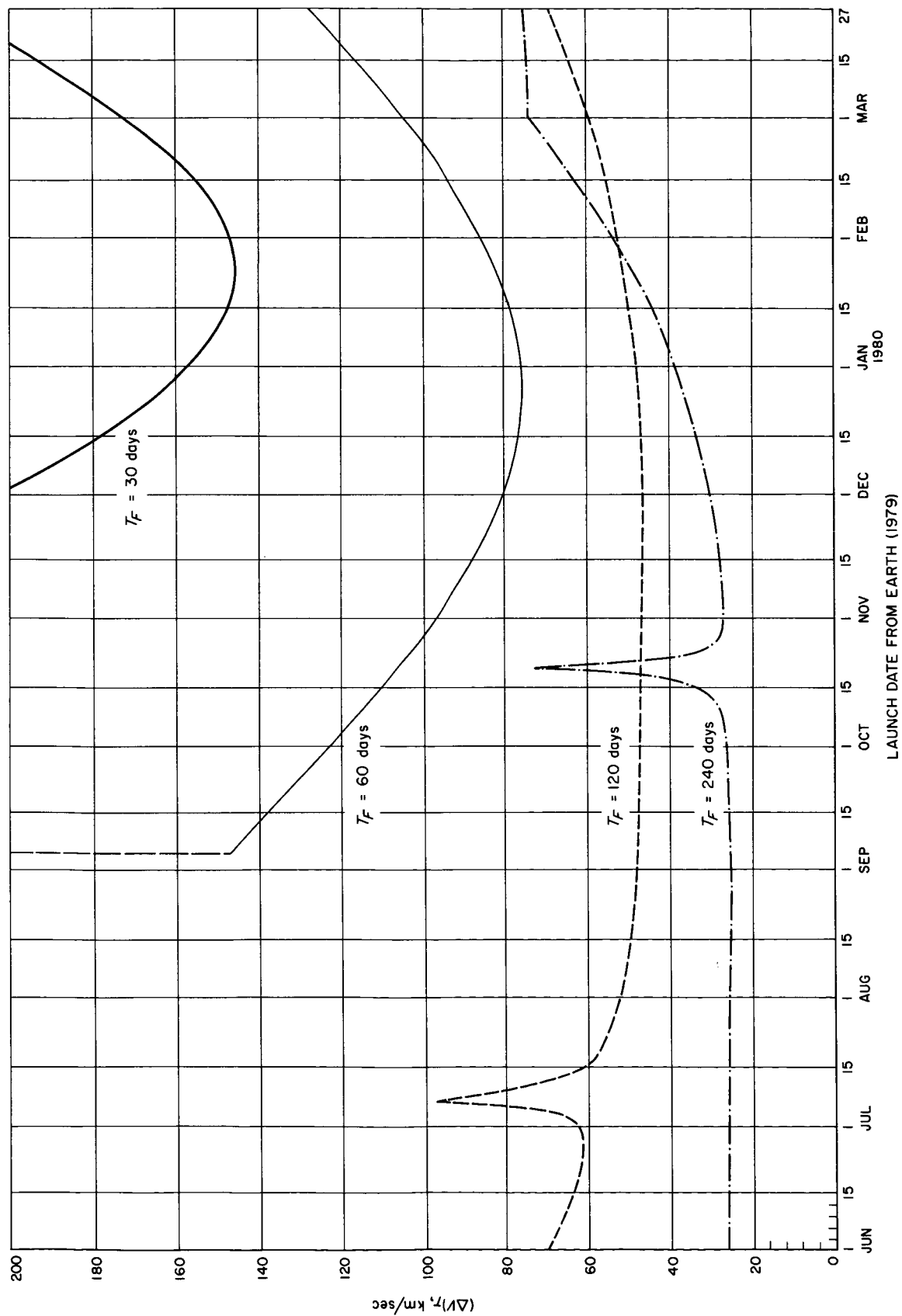


Fig. B-21. Earth-Mars-Earth trajectories, 1979, total speed increment from Earth orbit to Mars orbit to Earth orbit vs launch date

APPENDIX C

Tabulation of Reasons for Peculiar Variations in Plots of $(V_{\infty})_T$ and $(\Delta V)_T$ vs Launch Date From the Earth in the Decade 1970 to 1980

Table C-1. Reasons for the peculiar variations in Figs. B-2 through B-11 for the one-way time of flight of 30 days

Period in the 1970 decade	Launch date from the Earth	Figure	Type of variation	Reason for variation		Remarks
				Departure trajectory	Return trajectory	
1	Apr 30, '70	B-2	Small peak	Hyperbolic	Out-of-the-ecliptic hyperbolic	1. Out-of-the-ecliptic trajectories require higher energies than trajectories in or nearly in the ecliptic (see Section III-C). Planets are nearly in pseudo-conjunction for the return trajectory.
	Aug 28, '70	B-2	Small peak	Out-of-the-ecliptic hyperbolic	Hyperbolic	2. See remark 1. Note that in this case, the out-of-the-ecliptic trajectory occurs for the departure trajectory rather than for the return trajectory. Planets are nearly in pseudo-conjunction for the departure trajectory.
	Apr 13, '71	B-3	Discontinuity	Hyperbolic	Solution 1—Indirect, nearly rectilinear hyperbolic Solution 2—Direct, nearly rectilinear elliptic	3. The direct trajectory requires less energy than the indirect trajectory, since less distance must be traveled in the given time of flight (see Section III-B). Solution 1 is the higher-energy solution and is not shown in this Figure, as a result of the vertical scale. Planets are in pseudo-opposition for the return trajectory.
	Oct 5, '71	B-3	Discontinuity	Solution 1—Indirect, nearly rectilinear hyperbolic Solution 2—Direct, nearly rectilinear elliptic	Hyperbolic	4. See remark 3. Note that in this case the nearly degenerate trajectories occur for the departure trajectory rather than for the return trajectory. Planets are in pseudo-opposition for the departure trajectory.
	Jun 8, '72	B-4	Small peak	Hyperbolic	Out-of-the-ecliptic hyperbolic	5. See remark 1.
	Oct 2, '72	B-4	Small peak	Out-of-the-ecliptic hyperbolic	Hyperbolic	6. See remark 2.
	Jun 29, '73	B-5	Discontinuity	Hyperbolic	Solution 1—Indirect, nearly rectilinear hyperbolic Solution 2—Direct, nearly rectilinear elliptic	7. See remark 3.
	Dec 2, '73	B-5, B-6	Discontinuity	Solution 1—Indirect, nearly rectilinear hyperbolic Solution 2—Direct, nearly rectilinear elliptic	Hyperbolic	8. Owing to the scales of these Figures, the point of discontinuity is not shown. See remark 4.
	Jul 14, '74	B-6	Small peak	Hyperbolic	Out-of-the-ecliptic hyperbolic	9. See remark 1.
2						

3	Nov 11, '74	B-6	Small peak	Out-of-the-ecliptic hyperbolic	Hyperbolic	10. See remark 2.
	Sep 7, '75	B-7	Discontinuity	Hyperbolic	Solution 1—Indirect, nearly rectilinear hyperbolic Solution 2—Direct, nearly rectilinear elliptic	11. See remark 3.
	Jan 11, '76	B-7, B-8	Discontinuity	Solution 1—Indirect, nearly rectilinear hyperbolic Solution 2—Direct, nearly rectilinear parabolic	Hyperbolic	12. Owing to the scales of these Figures, the point of discontinuity is not shown. Solution 1 is nearly rectilinear parabolic, a rarity.
	Aug 20, '76	B-8	Small peak	Hyperbolic	Out-of-the-ecliptic hyperbolic	13. See remark 1.
4	Dec 31, '76	B-8	Small peak	Out-of-the-ecliptic hyperbolic	Hyperbolic	14. See remark 2.
	Oct 21, '77	B-9	Discontinuity	Hyperbolic	Solution 1—Indirect, nearly rectilinear hyperbolic Solution 2—Direct, nearly rectilinear elliptic	15. Owing to the vertical scale of this Figure the point of discontinuity is not shown. See remark 3.
	Feb 15, '78	B-9, B-10	Discontinuity	Solution 1—Indirect, nearly rectilinear hyperbolic Solution 2—Direct, nearly rectilinear hyperbolic	Hyperbolic	16. Owing to the vertical scale of this Figure the point of discontinuity is not shown. See remark 4. Note that both solutions are nearly rectilinear hyperbolic.
	Oct 5, '78	B-10	Small peak	Hyperbolic	Out-of-the-ecliptic hyperbolic	17. See remark 1.
5	Mar 11, '79	B-10	Small peak	Out-of-the-ecliptic hyperbolic	Hyperbolic	18. See remark 2.
	Nov 27, '79	B-11	Discontinuity	Hyperbolic	Solution 1—Indirect, nearly rectilinear hyperbolic Solution 2—Direct, nearly rectilinear elliptic	19. See remark 15. Note that both solutions are nearly rectilinear hyperbolic.
	Mar 17, '80	B-11	Discontinuity	Solution 1—Indirect, nearly rectilinear hyperbolic Solution 2—Direct, nearly rectilinear hyperbolic	Hyperbolic	20. See remark 16.

Table C-2. Reasons for the peculiar variations in Figs. B-2 through B-11 for the one-way time of flight of 60 days

Period in the 1970 decade	Launch date from the Earth	Figure	Type of variation	Reason for variation		Remarks
				Departure trajectory	Return trajectory	
1	Jan 28, '70	B-2	Small peak	Hyperbolic	Out-of-the-ecliptic hyperbolic	1. Out-of-the-ecliptic trajectories require higher energies than trajectories in or nearly in the ecliptic (see Section III-C). Planets are nearly in pseudo-conjunction for the return trajectory.
	Sep 22, '70	B-2	Small peak	Out-of-the-ecliptic hyperbolic	Hyperbolic	2. See remark 1. Note that in this case the out-of-the-ecliptic trajectory occurs for the departure trajectory rather than for the return trajectory. Planets are nearly in pseudo-conjunction for the departure trajectory.
	Jan 6, '71	B-2	Discontinuity	Hyperbolic	Solution 1—Indirect, nearly rectilinear hyperbolic Solution 2—Direct, nearly rectilinear elliptic	3. The direct trajectory requires less energy than the indirect trajectory, since less distance must be traveled in the given time of flight (see Section III-B). Solution 1 is the higher-energy solution. Planets are in pseudo-opposition for the return trajectory.
	Nov 17, '71	B-3, B-4	Discontinuity	Solution 1—Indirect, nearly rectilinear hyperbolic Solution 2—Direct, nearly rectilinear elliptic	Hyperbolic	4. Owing to the horizontal scale of this Figure, the point of discontinuity is not shown. See remark 3. Note that in this case the nearly degenerate trajectories occur for the departure trajectory rather than for the return trajectory. Planets are in pseudo-opposition for the departure trajectory.
	Mar 13, '72	B-4	Small peak	Hyperbolic	Out-of-the-ecliptic hyperbolic	5. See remark 1.
2	Oct 29, '72	B-4	Small peak	Out-of-the-ecliptic hyperbolic	Hyperbolic	6. See remark 2.
	Mar 6, '73	B-5	Discontinuity	Hyperbolic	Solution 1—Indirect, nearly rectilinear hyperbolic Solution 2—Direct, nearly rectilinear elliptic	7. See remark 3. Note that Solution 1 is not shown in this Figure, as a result of the vertical scale.
	Dec 31, '73	B-5, B-6	Discontinuity	Solution 1—Indirect, nearly rectilinear hyperbolic Solution 2—Direct, nearly rectilinear elliptic	Hyperbolic	8. See remark 4.
	Apr 20, '74	B-6	Small peak	Hyperbolic	Out-of-the-ecliptic hyperbolic	9. See remark 1.

3	Dec 14, '74	B-6	Small peak	Out-of-the-ecliptic hyperbolic	Hyperbolic	10. See remark 2.
	May 26, '75	B-7	Discontinuity	Hyperbolic	Solution 1—Indirect, nearly rectilinear hyperbolic Solution 2—Direct, nearly rectilinear elliptic	11. See remark 7.
	Feb 4, '76	B-8	Discontinuity	Solution 1—Indirect, nearly rectilinear hyperbolic Solution 2—Direct, nearly rectilinear elliptic	Hyperbolic	12. See remark 3. Note that in this case the nearly degenerate trajectories occur for the departure trajectory rather than for the return trajectory. Planets are in pseudo-opposition for the departure trajectory.
	May 26, '76	B-8	Small peak	Hyperbolic	Out-of-the-ecliptic hyperbolic	13. See remark 1.
4	Feb 16, '77	B-8	Small peak	Out-of-the-ecliptic hyperbolic	Hyperbolic	14. See remark 2.
	Jul 25, '77	B-9	Discontinuity	Hyperbolic	Solution 1—Indirect, nearly rectilinear hyperbolic Solution 2—Direct, nearly rectilinear elliptic	15. See remark 7.
	Mar 9, '78	B-9	Discontinuity	Solution 1—Indirect, nearly rectilinear hyperbolic Solution 2—Direct, nearly rectilinear elliptic	Hyperbolic	16. See remark 12. Note that solution 1 is not shown in this Figure, as a result of the vertical scale.
	Jul 5, '78	B-10	Small peak	Hyperbolic	Out-of-the-ecliptic hyperbolic	17. See remark 1.
5	Apr 29, '79	B-10	Small peak	Out-of the-ecliptic hyperbolic	Hyperbolic	18. See remark 2.
	Sep 5, '79	B-11	Discontinuity	Hyperbolic	Solution 1—Indirect, nearly rectilinear hyperbolic Solution 2—Direct, nearly rectilinear elliptic	19. See remark 7.
	Apr 14, '80	B-11	Discontinuity	Solution 1—Indirect, nearly rectilinear hyperbolic Solution 2—Direct, nearly rectilinear elliptic	Hyperbolic	20. See remark 16.

Table C-3. Reasons for the peculiar variations in Figs. B-2 through B-11 for the one-way time of flight of 120 days

Period in the 1970 decade	Launch date from the Earth	Figure	Type of variation	Reason for variation		Remarks
				Departure trajectory	Return trajectory	
1	Jul 14, '70	B-2	Double point	Elliptic	Changes from indirect, nearly rectilinear elliptic to direct, nearly rectilinear elliptic	1. The direct trajectory requires less energy than an indirect trajectory, since less distance must be traveled in the given time of flight (See Section III-B). Planets are nearly in pseudo-opposition for the return trajectory.
	Nov 14, '70	B-2	Small peak	Out-of-the-ecliptic elliptic	Elliptic	2. Out-of-the-ecliptic trajectories require higher energies than trajectories in or nearly in the ecliptic. (See Section III-C). Planets are nearly in pseudo-conjunction for the departure trajectory.
	Sep 10, '71	B-3	Small peak	Elliptic	Out-of-the-ecliptic elliptic	3. See remark 2. Note that in this case the out-of-the-ecliptic trajectory occurs for the return trajectory rather than for the departure trajectory. Planets are nearly in pseudo-conjunction for the return trajectory.
	Jan 14, '72	B-4	Double point	Changes from direct, nearly rectilinear elliptic to indirect, nearly rectilinear elliptic	Elliptic	4. See remark 1. Note that in this case the change in trajectory occurs for the departure trajectory rather than for the return trajectory. Planets are nearly in pseudo-opposition for the departure trajectory.
2	Aug 20, '72	B-4	Double point	Elliptic	Changes from indirect, nearly rectilinear elliptic to direct, nearly rectilinear elliptic	5. See remark 1.
	Jan 4, '73	B-4	Small peak	Out-of-the-ecliptic elliptic	Elliptic	6. See remark 2.
	Oct 29, '73	B-5	Small peak	Elliptic	Out-of-the-ecliptic elliptic	7. See remark 3.
	Feb 17, '74	B-6	Double point	Changes from direct, nearly rectilinear elliptic to indirect, nearly rectilinear elliptic	Elliptic	8. See remark 4.

3	Oct 12, '74	B-6	Double point	Elliptic	Changes from indirect, nearly rectilinear elliptic to direct, nearly rectilinear elliptic	9. See remark 1.
	Mar 16, '75	B-6, B-7	Small peak	Out-of-the-ecliptic elliptic	Elliptic	10. Owing to the horizontal scale of this Figure, the small peak is not shown. See remark 2.
	Dec 8, '75	B-7	Small peak	Elliptic	Out-of-the-ecliptic elliptic	11. See remark 3.
	Mar 23, '76	B-8	Double point	Changes from direct, nearly rectilinear elliptic to indirect, nearly rectilinear elliptic	Elliptic	12. See remark 4.
4	Dec 27, '76	B-8	Double point	Elliptic	Changes from indirect, nearly rectilinear elliptic to direct, nearly rectilinear elliptic	13. See remark 1.
	May 21, '77	B-8, B-9	Small peak	Out-of-the-ecliptic elliptic	Elliptic	14. See remark 10.
	Jan 13, '78	B-9	Small peak	Elliptic	Out-of-the-ecliptic elliptic	15. See remark 3.
	May 1, '78	B-10	Double point	Changes from direct, nearly rectilinear elliptic to indirect, nearly rectilinear elliptic	Elliptic	16. See remark 4.
5	Mar 6, '79	B-10	Double point	Elliptic	Changes from indirect, nearly rectilinear elliptic to direct, nearly rectilinear elliptic	17. See remark 1.
	Jul 9, '79	B-11	Small peak	Out-of-the-ecliptic elliptic	Elliptic	18. See remark 2.

Table C-4. Reasons for the peculiar variations in Figs. B-2 through B-11 for the one-way time of flight of 240 days

Period in the 1970 decade	Launch date from the Earth	Figure	Type of variation	Reason for variation		Remarks
				Departure trajectory	Return trajectory	
1	Mar 14, '70	B-2	Double point	Changes from an indirect, nearly rectilinear elliptic trajectory to a second indirect, nearly rectilinear elliptic trajectory	Elliptic	1. The double point exhibited on this launch day is caused by the change in the departure trajectory from an indirect, nearly rectilinear elliptic trajectory that passes by the secondary focus to an indirect, nearly rectilinear elliptic trajectory of lower energy that first passes by the Sun at the primary focus and then passes by the secondary focus (see Section III-B). Planets are nearly in pseudo-opposition for the departure trajectory.
	Jul 21, '70	B-2	Peak	Elliptic	Out-of-the-ecliptic elliptic	2. Out-of-the-ecliptic trajectories require higher energies than trajectories in or nearly in the ecliptic (see Section III-C). Planets are nearly in pseudo-conjunction for the return trajectory.
	May 7, '71	B-3	Peak	Out-of-the-ecliptic elliptic	Elliptic	3. See remark 2. Note that in this case the out-of-the-ecliptic trajectory occurs for the departure trajectory rather than for the return trajectory. Planets are nearly in pseudo-conjunction for the departure trajectory.
	Sep 19, '71	B-3	Double point	Elliptic	Changes from an indirect, nearly rectilinear elliptic trajectory to a second indirect, nearly rectilinear elliptic trajectory	4. The double point for this launch day is caused by the change in the return trajectory from an indirect, nearly rectilinear elliptic trajectory that first passes by the secondary focus and then passes by the Sun at the primary focus to an indirect, nearly rectilinear elliptic trajectory of higher energy that just passes by the secondary focus (see Section III-B). Planets are nearly in pseudo-opposition for the return trajectory.
2	Apr 18, '72	B-4	Double point	Changes from an indirect, nearly rectilinear elliptic trajectory to a second indirect, nearly rectilinear elliptic trajectory	Elliptic	5. See remark 1.
	Sep 12, '72	B-4	Peak	Elliptic	Out-of-the-ecliptic elliptic	6. See remark 2.

	Jun 28, '73	B-5	Peak	Out-of-the-ecliptic elliptic	Elliptic	7. See remark 3.
	Nov 1, '73	B-5	Double point	Elliptic	Changes from an indirect, nearly rectilinear elliptic trajectory to a second indirect, nearly rectilinear elliptic trajectory	8. See remark 4.
3	Jun 7, '74	B-6	Double point	Changes from an indirect, nearly rectilinear elliptic trajectory to a second indirect, nearly rectilinear elliptic trajectory	Elliptic	9. See remark 1.
	Nov 23, '74	B-6	Peak	Elliptic	Out-of-the-ecliptic elliptic	10. See remark 2.
	Aug 7, '75	B-7	Peak	Out-of-the-ecliptic elliptic	Elliptic	11. See remark 3.
	Nov 26, '75	B-7	Double point	Elliptic	Changes from an indirect, nearly rectilinear elliptic trajectory to a second indirect, nearly rectilinear elliptic trajectory	12. See remark 4.
4	Aug 19, '76	B-8	Double point	Changes from an indirect, nearly rectilinear elliptic trajectory to a second indirect, nearly rectilinear elliptic trajectory	Elliptic	13. See remark 1.
	Jan 26, '77	B-8	Peak	Elliptic	Out-of-the-ecliptic elliptic	14. See remark 2.
	Sep 12, '77	B-9	Peak	Out-of-the-ecliptic elliptic	Elliptic	15. See remark 3.
	Jan 7, '78	B-9	Double point	Elliptic	Changes from an indirect, nearly rectilinear elliptic trajectory to a second indirect, nearly rectilinear elliptic trajectory	16. See remark 4.
5	Nov 1, '78	B-10	Double point	Changes from an indirect, nearly rectilinear elliptic trajectory to a second indirect, nearly rectilinear elliptic trajectory	Elliptic	17. See remark 1.
	Mar 14, '79	B-10	Peak	Elliptic	Out-of-the-ecliptic elliptic	18. See remark 2.
	Oct 20, '79	B-11	Peak	Out-of-the-ecliptic elliptic	Elliptic	19. See remark 3.
	Mar 1, '80	B-11	Double point	Elliptic	Changes from an indirect, nearly rectilinear elliptic trajectory to a second indirect, nearly rectilinear elliptic trajectory	20. See remark 4.